5-2010

SYSTEM MODELING AND POWER MANAGEMENT STRATEGY FOR A SERIES HYDRAULIC HYBRID VEHICLE

Sisay Molla
Clemson University, smolla@clemson.edu

SYSTEM MODELING AND POWER MANAGEMENT STRATEGY FOR A SERIES HYDRAULIC HYBRID VEHICLE

A Thesis
Presented to
the Graduate School of
Clemson University

In Partial Fulfillment
of the Requirements for the Degree of
Master of Science in
Mechanical Engineering

---

by
Sisay Kefyalew Molla
May 2010

Accepted by:
Dr. Beshah Ayalew, Committee Chair
Dr. Ardalan Vahidi
Dr. Harry Law

ABSTRACT

A hydraulic hybrid vehicle draws propulsion power from an internal combustion engine as its prime mover and a gas-charged hydro-pneumatic accumulator as its energy buffer. The accumulator serves the purposes of storing regenerated braking energy and supplementing engine power as determined by an on-board power management strategy. In the configuration known as a series hydraulic hybrid powertrain, the engine is mechanically decoupled from the vehicle's wheels thereby offering excellent opportunities for maximizing energy efficiency and reducing pollutant emissions.

This thesis dealt with the development of a causally interconnected, non-linear, dynamic model of a series hydraulic hybrid powertrain featuring independently controllable wheel-end drives. Using the model so developed, the work investigated the potentials of three proposed power management strategies on the fuel/energy use of a test vehicle. The strategies studied included: a real-time implementable rule-based strategy, an on-line solvable instantaneous consumption minimization strategy, and a non-causal trip/globally optimal power management strategy based on dynamic programming.

The results indicated that, when properly designed, all three power management strategies can help realize the fuel economy benefits of the proposed hydraulic hybrid drive system. Over a standard city drive cycle, the rule-based power management strategy was shown to provide a fuel economy improvement of more than 30% with four-motor drive over the conventional drive system. The trip/globally optimal strategy obtained via dynamic programming gave an average of over 50% higher fuel economy improvement

with four-motor drive. The instantaneous consumption minimization strategy, which is adopted to overcome the non-causality of dynamic programming and the lack of rigorous optimality of the rule-based strategy, gave fuel economy improvements that generally fell between the other two strategies. Results are also included from the analysis of the effects of accumulator size and two-motor vs. four motor drive options along with the choice of the power management strategy.

DEDICATION

This thesis is dedicated to my family: my parents, Almaz Abera and Kefyalew Molla, my sister Alem Molla and my brothers Hailemichael and Habtamu Molla.

ACKNOWLEDGEMENT

I would like to thank my research advisor Dr. Beshah Ayalew for his guidance, encouragement and continuous support throughout my graduate study. I would also like to thank Dr. Ardalan Vahidi and Dr. Harry Law for their willingness to give of their time and expertise in serving as my committee members and evaluating my thesis.

Finally, I acknowledge the financial support provided through the Automotive Research Center, A U.S. Army Center of Excellence for Modeling and Simulation of Ground Vehicles led by the University of Michigan.

TABLE OF CONTENTS

LIST OF TABLES

LIST OF FIGURES

CHAPTER ONE

1 INTRODUCTION

1.1 Background and Motivation

Concerns about resource depletion and climate change have accelerated the exploration of alternative and energy efficient vehicle propulsion systems. Some of these proposed alternatives are hybrid vehicles. In general, a hybrid vehicle is defined as a vehicle having two or more on-board propulsion energy sources - usually an internal combustion engine or a fuel cell as a prime mover and one or more energy storage devices (batteries, ultracapacitors, flywheels or accumulators) as energy buffers.

The apparent advantages of hybrid vehicles are:

- ***Improved fuel economy***: A hybrid powertrain has the potential to significantly improve fuel economy for vehicles especially in urban driving cycles characterized by frequent stop-and-go motion. This is accomplished by: 1) storing the fraction of the kinetic energy of the vehicle during braking (regenerative braking) in the energy buffers and using the stored energy to propel the vehicle during subsequent acceleration or cruising; 2) exploiting the mechanical decoupling of the engine from the drive wheels (the road load) and controlling the engine to operate near its most efficient operating points on its torque-speed map and/or turning it off when it is not required (e.g. when idling); 3) running the

vehicle accessories at more efficient points by decoupling them from the engine speed [1-3].

- ***Reduce emission:*** In addition to reduced green house gas emissions achieved from reduced fuel consumption, due to the fact that engine decoupling is realizable, it is possible to control the engine where complete combustion is possible or in a manner that favors emission reduction schemes [4].
- ***Reduce wear of brake-linings:*** Regenerative braking reduces the activation of friction brakes to stop or retard the vehicle which certainly reduces the wear of brake-linings and hence the associated cost of replacement/maintenance [4].
- ***Performance improvement*****:** Hybrid vehicles have the potential to improve the acceleration and grade-ability performance of the vehicle through combined engine power and stored power delivered by the storage unit or to reduce engine size without deteriorating the performance of the vehicle [5, 6].
- ***Regenerative- or Traction-based lateral vehicle stability control*****:** In the case of series hybrid vehicles, independently controlled (electric or hydraulic) motors can be mounted at or near the vicinity of the wheels of the vehicle so that when braking is required at each one of the vehicles' wheels for lateral stability control, the motors can work as a generator or a pump thereby regenerating energy onto the on-board storage unit while simultaneously stabilizing the vehicle. It is also possible to enable a traction (drive)-based lateral stability control by using the independently controlled motors [7-10].

In the past few decades, most research and development on hybrid powertrains has focused almost exclusively on electric hybrid vehicles. By comparison, little effort has been expended on hydraulic hybrids [11, 12]. Recently, hydraulic hybrid drives are drawing increased attention, especially for heavy –and medium –duty vehicles that have use cycles characterized by frequent stop-and-go [5, 13, 14]. The reasons for this increased attention are the following positive attributes of hydraulic hybrids as compared to electric hybrids:

- Hydraulic machines have inherently high-power density (peak power per unit mass) as compared to their electric counterparts. This is important for accommodating and releasing high power during sudden braking and acceleration without adding too much mass to the vehicle. It also opens up the possibility of using multiple but smaller pumps/motors for a per-axle or per-wheel drive arrangement [6, 7].
- The round-trip energy storage and release efficiency of hydraulic accumulators (storage) is generally better than that of electric batteries. For instance, the round trip efficiency of a bladder type hydro-pneumatic accumulator with elastomeric foam reaches up to 95% [15] and can accept high charging and discharging rates, both of which are not favorable to electro-chemical batteries due to their chemical reaction limitations [2, 15, 16].
- Hydraulic components (pumps, motors, accumulators) are relatively inexpensive when compared with their electric counterparts, especially the advanced battery

packs [13], electric machines and their required power electronics (DC to DC convertors, inverters, etc.).

The combination of the high power density of hydraulic pump/motors (P/M), the high efficiency and high charging and discharging rates of hydro-pneumatic accumulators expedite successful regeneration and re-use of energy [15]. However, hydraulic accumulators exhibit relatively low-energy density. This necessitates a great deal of attention on the design of higher level power management strategies for exploiting the full benefits of the hydraulic hybrid drivetrain under this constraint imposed by the accumulators [15, 16].

A carefully design and optimized power management strategy could leverage the high power density of the hydraulic energy storage system while maximizing the efficiency of the overall hybrid drive. Usually, an internal combustion engine generates power most efficiently when operating in a narrow regime near the peak torque curve of the engine. Operating at other conditions diminishes its energy conversion efficiency. Therefore, a good hybrid power management strategy would consider this into account and run the engine near the peak efficiency regime by taking or storing the balance of propulsion power in the accumulator [13].

1.2 System Configurations

Hydraulic hybrid powertrain arrangements can be readily classified into three basic categories based on their configurations: the pure hydrostatic systems (also known

as series hydraulic hybrid vehicles), the hydro-mechanical systems (parallel hydraulic hybrid vehicles), and the hydrostatic power split systems.

The series hydraulic hybrid vehicle design, shown in Figure 1-1, removes the conventional transmission and drive shaft. The hydraulic pump, which is mechanically connected to the engine, converts the mechanical power output of the engine to hydraulic power. The high-pressure hydraulic fluid then either charges the accumulator or directly flows to the pump/motor at the wheel-end to propel the vehicle. This arrangement allows the vehicle's ground speed and the engine speed to be decoupled. This in turn permits the engine to be controlled at its best efficiency regime in its torque-speed map. In addition, when braking is initiated or the vehicle comes to a complete stop, the engine may be turned off.

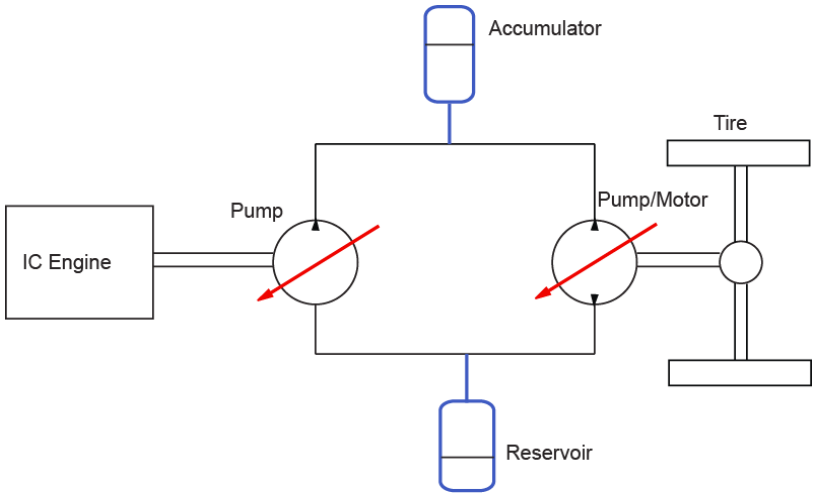

Figure 1-1 Series hydraulic hybrid (pure hydrostatic) system configuration

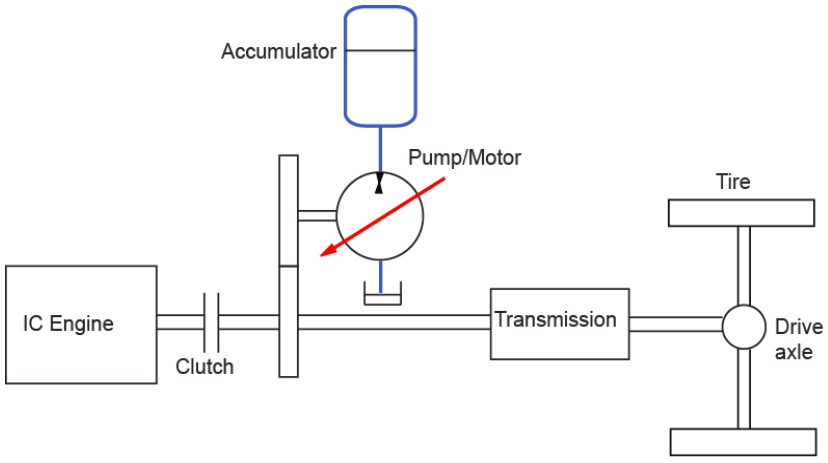

Figure 1-2 Parallel hydraulic hybrid (hydro-mechanical) system configuration

The hydro-mechanical (parallel) powertrain design, shown in Figure 1-2, keeps the conventional transmission and driveshaft system unchanged while an additional hydraulic pump/motor unit is attached in parallel to the mechanical path to absorb and/or deliver a hydraulic power from/to the mechanical system. The design does not decouple the engine speed from the ground speed and hence doesn't permit the engine to be controlled at its best efficiency regime. However, when the relative sizing is such that significant power is transmitted through the more efficient mechanical transmission (compared to the hydrostatic path), the overall fuel economy of the hydro-mechanical powertrain may be better than a series one for some drive cycles. [3, 5, 13]

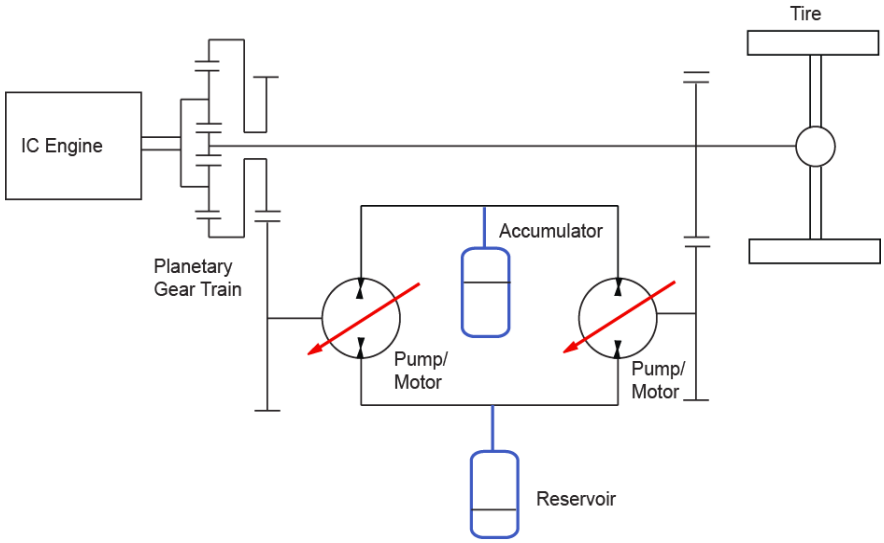

Figure 1-3 Power split hydraulic hybrid vehicle system configuration

The power split powertrain design, shown in Figure 1-3, combines the convenience of pure hydrostatic powertrain (the possibility of running the engine at its most efficient points) with the high overall transmission efficiency of the hydro-mechanical powertrain using the planetary gear train arrangement so that it offers the advantages of both layouts while minimizing their drawbacks [4, 5, 14].

1.3 Hybrid Power Management Strategies

The power management strategy of a hybrid vehicle is very crucial to achieve better fuel economy and lower emission without deteriorating the performance of the vehicle in other aspects such as acceleration. The benefits of hybrid vehicles are realizable to the fullest if they include a well-developed power management strategy that determines the power split between the two or more power sources.

Different types of energy management strategies have been discussed in the literature [17-22]. However, almost all of those power management strategies can be grouped under one of the following three categories.

The first group of approaches use control algorithms such as heuristic rules or fuzzy logic for estimation and control of the hybrid arrangements [19, 22-25]. The underlying concept for the extraction of the rules is the concept of “load-leveling”. It considers the use of irreversible energy source, like ICE, as the primary energy source to supply the power request from the driver and a reversible power source (Accumulator/battery/flywheel/supper capacitor) to act as a load-leveling device to supplement the rest of the power request.

The second approach is based on instantaneous point-wise optimization method. In this method, the power from the reversible energy storage device is converted to an equivalent fuel use rate in order to calculate the overall fuel cost at each instant of time. Then, for a known state and power demand, the control law is chosen in such a way that this equivalent fuel use is minimized without violating the constraints [21, 26-28].

The third type of control strategy considers the optimization of the dynamic allocation of the power split between the two on-board sources over a specified time horizon [14, 18, 27, 29, 30]. This type of control strategy gives more accurate results under transient conditions. However, it is more computationally intensive and this makes it generally infeasible for real time implementations [20].

1.4 Contribution of the Thesis

This thesis investigated the potential use of a series hydraulic hybrid vehicle equipped with four independently controlled pump/motors for fuel economy and longitudinal performance improvement. The tasks accomplished in this thesis were the following:

- Developed a full, causally interconnected, and nonlinear dynamic model of the powertrain for a series hydraulic hybrid vehicle (SHHV) for the purpose of system level simulations and analyses;
- Developed three power management strategies and implemented them in system simulations for select drive cycles and compared the fuel economy and performance improvements achieved with the SHHV. The first is a heuristic rule-based strategy and the other two were based on an optimization framework involving dynamic programming and instantaneous optimization techniques.
- Utilized the system model to study the effects of accumulator size selection on the fuel economy achieved with the SHHV and particular power management strategies.

The purpose of the dynamic model is to accurately simulate and predict the behavior of all of the components of the independent hydrostatic wheel drive system and trace out the effect of each component on the fuel economy improvement and the longitudinal performance of the vehicle. This model could also be used in the design of the complete powertrain (e.g. selecting and matching components) for an SHHV by evaluating the system performance over different drive cycles.

The dynamic system model developed in this thesis was also integrated in a lateral vehicle dynamics model for the purpose of investigating the use of the hydrostatic system with independently controlled wheel motors in enhancing the lateral stability of the vehicle. The author and his co-authors have documented this aspect in the two papers [7, 31].

1.5 Thesis Outline

The thesis is organized as follows. Chapter 2 starts with a description of the proposed independent hydrostatic wheel drive system. It then details the system and subsystem models adopted, i.e, the mathematical models of the hydrostatic powertrain components, the IC engine and the longitudinal vehicle dynamics and the strict physical causality (sub-system input-output relationships) adopted for proper integration. The hydrostatic powertrain component models include that of the hydraulic pumps/motors, the accumulator/reservoir, the hydraulic transmission lines and junctions.

Chapter 3 presents the general structure of hybrid power management strategy and discuses the main functions of the system supervisory controller for the proposed hydrostatic powertrain. It reviews the different types of power management strategies that have been adopted for this study and it details, the formulation and implementation of the rule-based power management strategy. This chapter also presents the effect of accumulator size and number of propulsion motors on the achievable fuel economy improvement.

Chapter 4 presents the derivation and implementation of the two optimization-based power management strategies applied to the hydrostatic (series hydraulic hybrid) powertrain. The chapter begins by discussing the dynamic programming (DP) algorithm for searching the optimal control laws by minimizing the given cost function and generate the globally optimal solution for a given/known drive cycle. Then the second type of optimization based power management strategy, the instantaneous equivalent consumption minimization strategy (ECMS), is presented in depth. The working principle and implementation of this strategy is presented first, followed by a discussion of the predicted fuel economy improvements.

Chapter 5 presents and discusses results comparing the three power management strategies. The fuel economy improvements obtained by rule-based, DP algorithm and ECMS strategy are considered side by side, compared and analyzed.

Finally, Chapter 6 summarizes the conclusions of the work and highlights directions for further research.

CHAPTER TWO

2 DYNAMIC SYSTEM DESCRIPTION AND MODELING

This chapter describes the complete system in detail and outlines the modeling of the main components of the hydrostatic powertrain, including reduced-order engine dynamics and the longitudinal vehicle dynamics. A carefully understood system interaction and constructed model is crucial for simulating the actual behavior of the vehicle in order to evaluate the impact of different power management strategies and main powertrain component sizes on the achievable fuel economy improvement, drivability and vehicle stability control algorithms.

2.1 System Description

The schematic representation of the series hydraulic hybrid system featuring independent hydrostatic wheel drives is shown in Figure 2-1. It includes an internal combustion engine (ICE) driven pump, high pressure and low pressure accumulators, transmission lines and four individual wheel-end pump/motors. The ICE is directly connected to a variable displacement pump which converts the mechanical power of the engine into hydraulic power. The high pressure fluid from the pump either charges the high pressure accumulator or directly flows to the individual wheel-end pump/motors (P/M). The ICE can be turned off to improve system efficiency when the vehicle comes to a full stop or when the power management strategy controller commands engine turn-off. The wheel-end P/Ms can be operated either as motors in drive mode or as pumps

during regenerative braking and/or when a vehicle stability control system dictates the specific mode of operation.

The hydrostatic powertrain system is defined as having one power producing unit (engine) and three power producing/consuming units (engine-pump, accumulator and wheel-end pump/motors). A basic power flow diagram of these system components and the associated system efficiency are shown in Figure 2-2. This figure shows the power flow sign convention adopted throughout this thesis. The power into the accumulator (charging) is taken as positive whereas, power out from the accumulator (discharging mode) is taken as negative. The power output of the hydraulic pumps/motors (engine side pump and wheel-end pumps/motors) working as a pump mode is taken as positive. Conversely, the power input to the hydraulic pumps/motors working as a motor mode (driving mode) is taken as negative. The system control boundary shows that accumulator input and output power is considered internal to the system as a result the power use of accumulator has no cost associated with it. Whereas, the fuel use of the engine and the demand power at the wheels of the vehicle crosses the boundary as input and input/output of the system respectively.

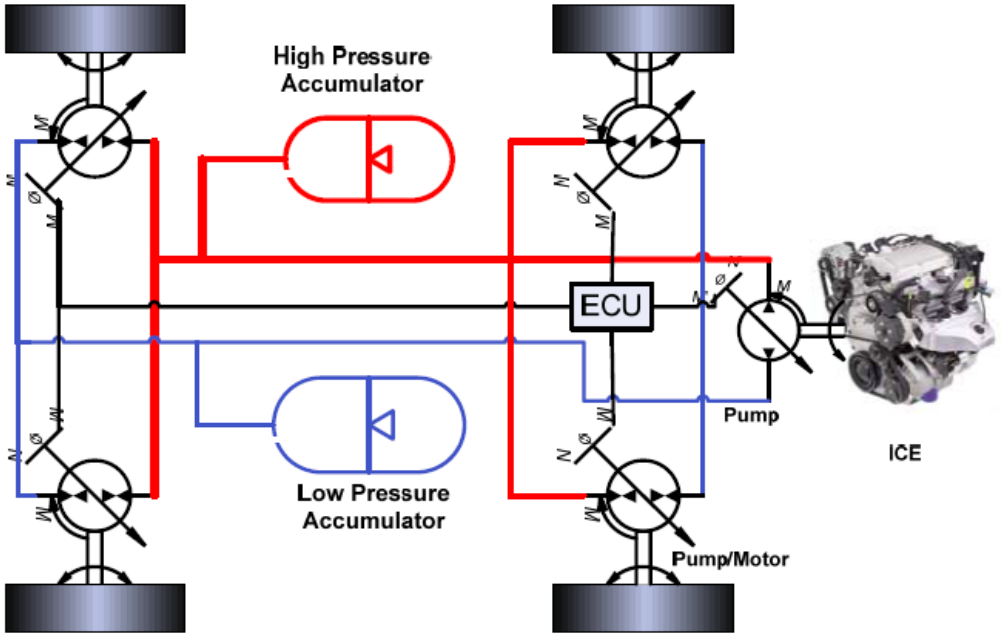

Figure 2-1 Schematic of 4X4 independent hydrostatic wheel drive

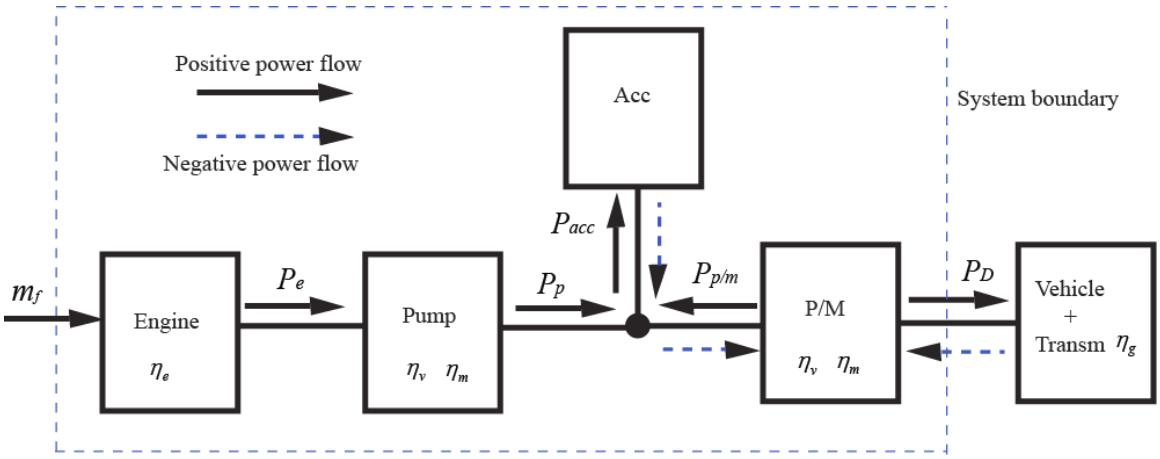

Figure 2-2 System efficiency and power flow diagrams of a series hydraulic hybrid vehicle

2.2 System Modeling

2.2.1 Higher Level Model Structure

The high-level system model architecture comprising of the engine and hydrostatic powertrain subsystems, the supervisory controller, the driver and vehicle dynamics subsystems, is depicted in Figure 2-3. The individual components of each of these subsystems are developed on the basis of forward-facing models interconnected by enforcing strict physical causality that emulates the physical manifestation of the real system.

The adopted causal interconnections between the subsystems are shown in Figure 2-4. Here, the input to the accumulator model is the oil flow rate from the junction through the orifice and the gas pressure is the response from of the accumulator model. The accumulator pressure through the orifice is then enforced on the junction, and subsequently on the wheel-end pump/motors (P/M) and the engine-side pump. Likewise, the vehicle speed dictates the wheel-end P/M speed and subsequently the flow rate into the junction from the wheel-end P/M unit. The junction is a summing point for the flow rates into/from the accumulator, the engine-side pump and the wheel-end P/M. The details of each of the component models are outlined in the following subsections.

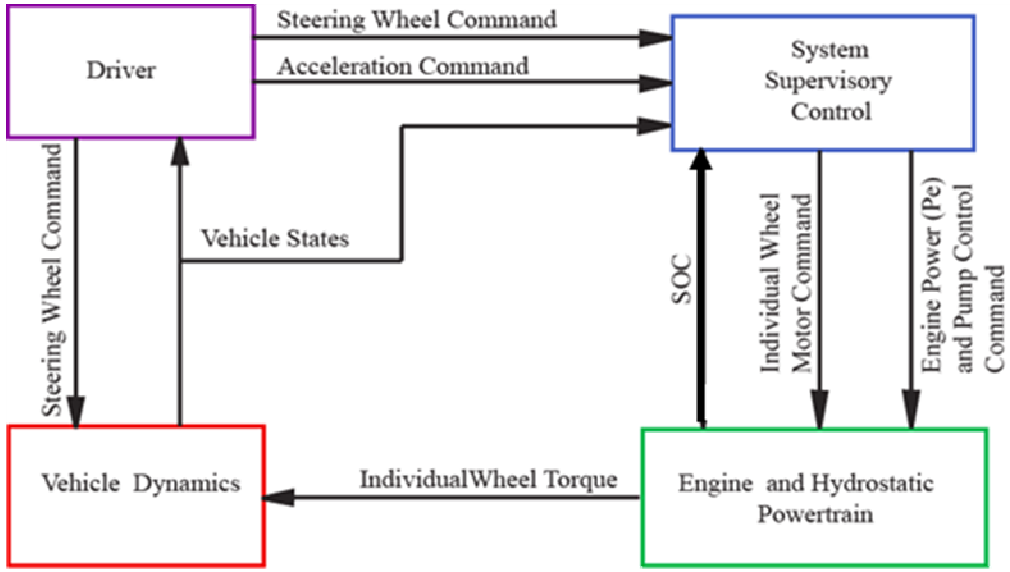

Figure 2-3 High-level system model architecture

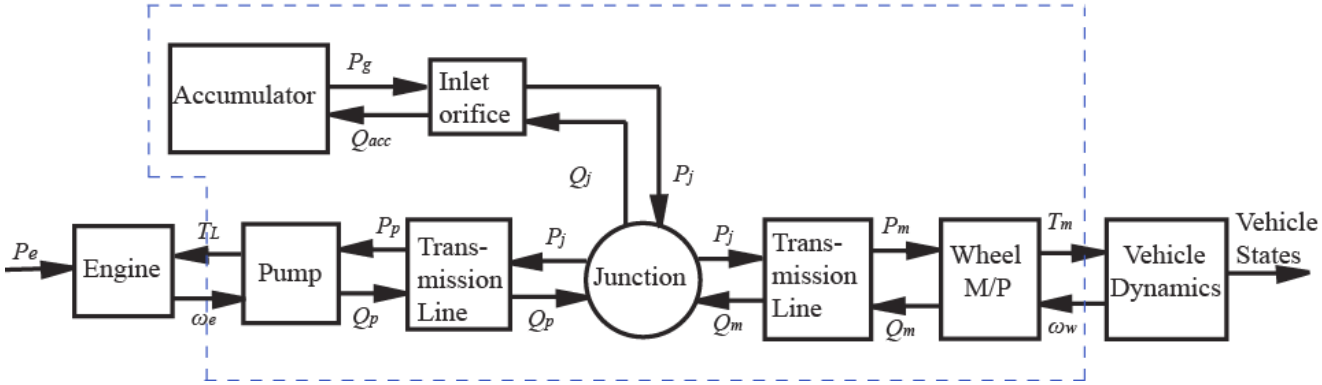

Figure 2-4 Casual interconnection of hydrostatic powertrain component model

2.2.2 Hydrostatic Powertrain Mode

The model for the hydrostatic powertrain subsystem includes models for the pump/motor, accumulator, reservoir (low pressure accumulator), junction and hydraulic transmission lines. The subsystem itself connects the engine and the vehicle dynamics model as shown in Figure 2-4. The inputs to the subsystem are the engine speed and the rotational speed of the wheels from the engine and from the vehicle dynamics subsystems, respectively. The outputs are the load torque and motor torque to the engine and to the wheels, respectively.

2.2.2.1 Pump/Motor Model

The main components of a hydrostatic transmission are hydraulic pumps and motors, which convert mechanical power to fluid power or vice versa. As can been seen by the causality of the P/M unit in Figure 2-4, the hydrostatic pump/motors do not create pressure, rather they create flow and the pressure results from a restriction or resistance to this flow. This is normally the work accomplished by the pump/motor unit.

The 4 pump/motors (P/Ms) considered are of the bent-axis design and are mechanically coupled to the wheels of the vehicle through a speed-reducing gearbox. The P/M units convert available hydraulic power from the engine-driven pump or the accumulator into mechanical power for vehicle propulsion (in motor mode), or convert some of the kinetic energy of the vehicle to hydraulic energy for storage in the accumulator during regenerative braking (in pump mode). Either the motor or pump

mode can be activated for the P/M units individually to generate a prescribed corrective yaw moment for vehicle stability control.

The P/M units (either at the engine or the wheel-end) are modeled here based on 3-D look-up tables of measured steady-state efficiency data. A schematic of the model structure is shown in Figure 2-5. The torque and the flow rate through the variable displacement P/M are functions of, and can be controlled by, the displacement factor, x, which is defined as the ratio of the prevailing displacement to the maximum displacement of the machine.

The relationship given by the look-up tables are denoted as functions $\eta(x, \omega, \Delta p)$ where the arguments (inputs) are x, ω, and Δp across the P/M unit and the volumetric efficiency η_v and the mechanical efficiency η_m of the P/M unit are interpolated for as outputs. Knowing these efficiency values, the flow rate and the torque of the P/M can be computed by using the following sets of equations, which also define the causal-relationships adopted for the P/M unit. This look-up table approach avoids the need for the numerous dimensionless numbers and loss coefficients frequently used in pump/motor modeling following Wilson's pump theory [4, 32-34].

$$Q_a = x\omega D\eta_v^{\pm 1}(x, \omega, \Delta p) \quad \textbf{(2.1)}$$

$$T_a = \frac{x\Delta P D}{\eta_m^{\mp 1}(x, \omega, \Delta p)} \quad \textbf{(2.2)}$$

where the $\pm$ signs on the superscripts correspond to the pump (+) or motor (-) modes of operations for the P/M unit under consideration. These equations are verified by the fact that for a pump the actual volumetric flow rate is lower than the ideal volumetric

flow rate due to leakage and fluid compressibility. On the other hand, the actual torque required to operate the pump is greater than the ideal one (determined by the differential pressure across the machine and its displacement) due to inevitable frictional losses. The opposite is true in the case of motor mode of operation for the P/M unit.

The rotational speed dynamics for the motors is coupled with the vehicle dynamics through the tire-wheel dynamics; a gear reduction and a driver model (see the next section below).

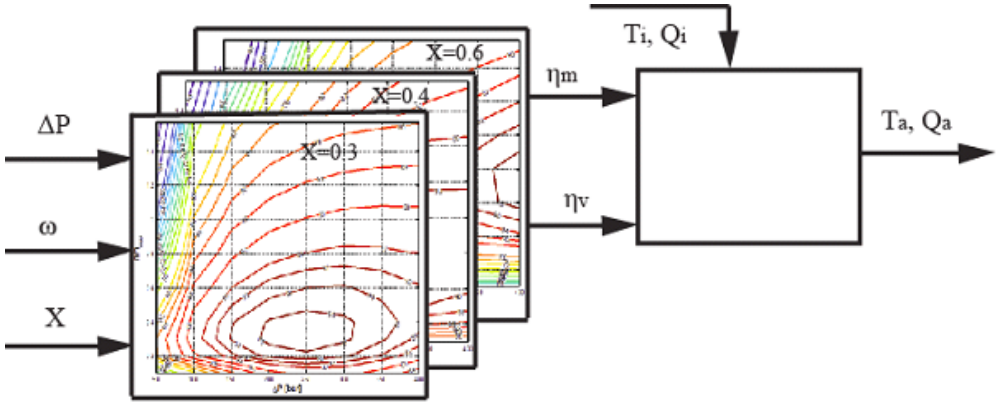

Figure 2-5 Steady state based look up table modeling of pumps and motors

The total efficiency ($\eta_t = \eta_m \eta_v$) map of the wheel-end P/M unit, as a function of speed ratio (n/n_{max}: the ratio of the current speed to the maximum speed of the P/M) and change in pressure across the P/M unit (Δp) for different values of displacement factor (x), is plotted in Figure 2-6. The plot shows the influence of each of the input variables on the efficiency of the P/M. For example, as the displacement factor of the P/M is increased, say from 0.3 to 0.8, the maximum available efficiency of the unit increases from 75% to 93%. This is consistent with the notion that higher displacement is favorable

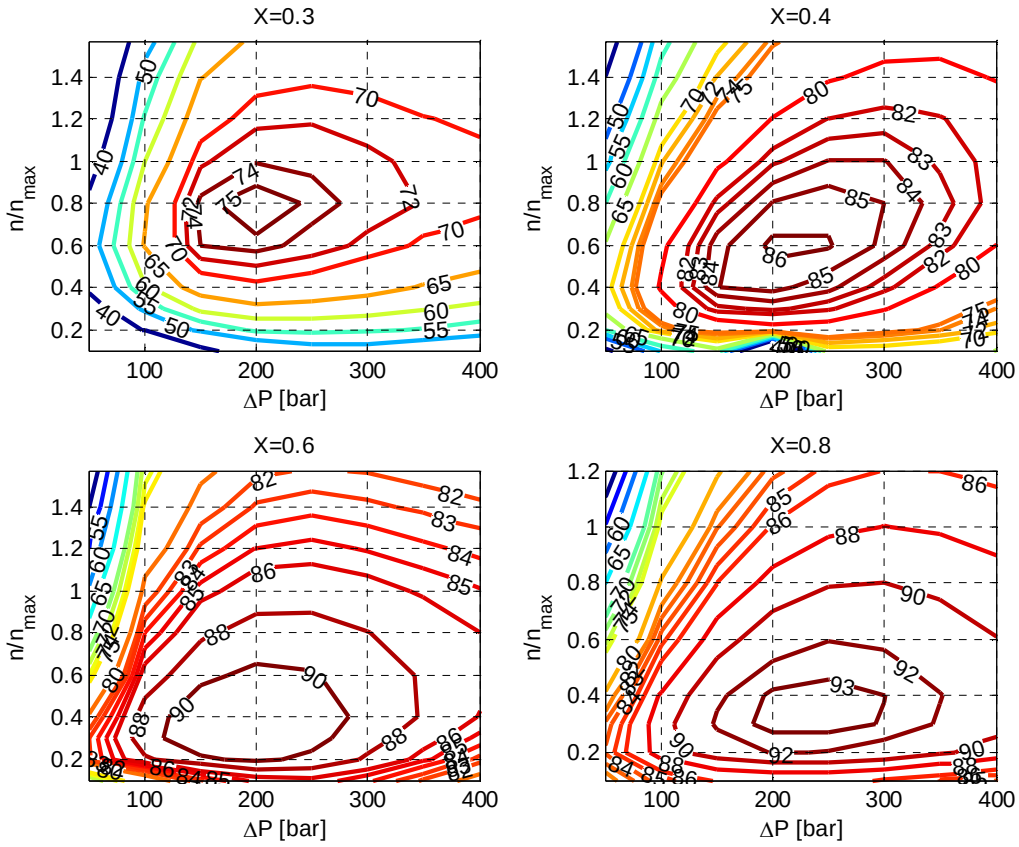

Figure 2-6 Total efficiency plots of the P/Ms as a function of speed ration and pressure difference across the P/M at a fixed pump displacement

to the better efficiency operation of the machine. For a fixed displacement factor, say x=0.8, and at low discharge pressure and very high pump speed, around the maximum speed of the pump, the efficiency becomes very low. This is due to increase in viscous friction losses that are proportional to the rotational speed of the pump. On the other hand, at low speed, and high Δp the efficiency deteriorates as the leakage and compressibility of the fluid increase. The efficiency also slightly deteriorates at high Δp and speed since each of the factors viscous friction, leakage, and compressibility become significant. We can see that there is a "sweet-spot" for efficiency of the P/M unit in the

middle of the operating range and top efficiency increases as the displacement of the machine is increased.

2.2.2.2 Accumulator/Reservoir Model

An accumulator is a pressure vessel that contains a hydraulic fluid and a pressurized inert gas (mostly nitrogen) where the two sides are separated by a bladder, a diaphragm or a piston, Figure 2-7. When hydraulic fluid is pumped in, the gas is compressed, causing its pressure to increase and store energy. When the fluid is discharged through the P/M (in motor mode), the pressure in the gas decreases while delivering propulsion energy. A reservoir (or low pressure accumulator) is a hydraulic accumulator working at much lower pressure that is just enough to prevent the occurrence of cavitation in the P/M units [22].

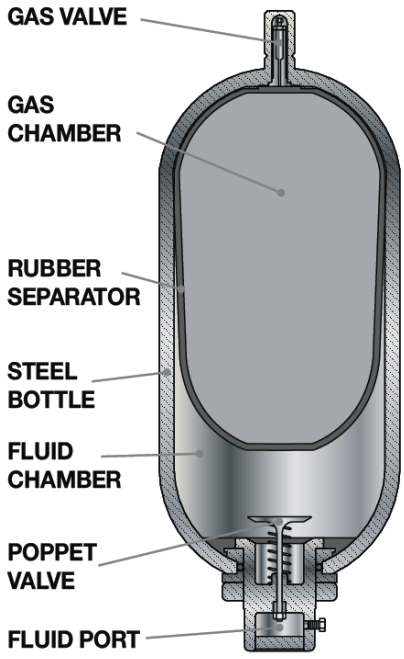

Figure 2-7 Sectional view of bladder type hydraulic accumulator/reservoir [35]

Detailed modeling of hydraulic accumulators has been undertaken earlier by Pourmovahed [36]. The suitable casualty of the system is shown in Figure 2-4 where the input is the accumulator flow rate through its orifice and the output is the gas pressure. Considering the use of elastomeric foam on the gas side of the accumulator (to reduce irreversible heat losses) and taking energy balance on the gas side, it can be shown that the temperature evolution is given by [36, 37]

$$\left[1+\frac{m_f c_f}{m_g c_v}\right]\frac{dT}{dt}=\frac{T_w-T}{\tau}-\frac{T}{c_v}\left(\frac{\partial p_g}{\partial T}\right)_v\frac{dv}{dt} \qquad \textbf{(2.3)}$$

where τ is the average thermal time constant, which is defined as $\tau=\frac{m_g c_v}{hA_w}$, with an average effective wall area, A_w, and convective heat transfer coefficient, h. The pressure in the accumulator is related to the gas temperature and the specific volume through a real-gas equation of state, such as the Beattie-Bridgeman (BB) equation of state [38]:

$$p_g=\frac{RT(1-\varepsilon)}{v^2}+\left(v+B\right)-\frac{A}{v^2} \qquad \textbf{(2.4)}$$

where, $A=A_0(1-a/v)$, $B=\frac{B_0(1-b)}{v}$, $\varepsilon=\frac{c}{vT^3}$ and A_0, B_0, a, b, c are constants in the BB equation of state. The specific volume (v) of the gas is related to the accumulator flow rate (Q_{acc}) as:

$$\frac{dv}{dt}=\frac{-Q_{acc}}{m_g} \qquad \textbf{(2.5)}$$

With,

$$
\begin{aligned}
Q_{acc} &= \sum_{i=1}^{n} Q_{p/m,i} + Q_p \\
&= \sum_{i=1}^{n} \left[x_{p/m,i} D_{p/m,i} \omega_{p/m,i} \eta_{v,i}^{\pm 1}(x_{p/m,i}, \omega_{p/m,i}, \Delta p_{p/m,i}) \right] + x_p D_p \omega_p \eta_v(x_p, \omega_p, \Delta p_p)
\end{aligned}
\tag{2.6}
$$

The first term on the right side of Eq. (2.6) is the sum of the individual (*i=1: n*) flow rates to/from the P/Ms, considered positive in pump mode. And the second term is the flow rate from the engine-driven pump, also positive in pump mode. The hydraulic fluid flow rate into the accumulator (charging) is taken as positive. The state of charge (SOC) of the accumulator is defined as the ratio of the instantaneous oil volume in the accumulator to the maximum possible oil capacity and is given by:

$$
\begin{aligned}
SOC &= \frac{\int_{V_0}^{V} Q_{acc} dt}{V_{acc}} \\
&= \frac{\int_{V_0}^{V} \left(\sum_{i=1}^{n} \left[x_{p/m,i} D_{p/m,i} \omega_{p/m,i} \eta_{v,i}^{\pm 1}(x_{p/m,i}, \omega_{p/m,i}, \Delta p_{p/m,i}) \right] + x_p D_p \omega_p \eta_v(x_p, \omega_p, \Delta p_p) \right) dt}{V_{acc}}
\end{aligned}
\tag{2.7}
$$

Measuring the instantaneous oil volume is not straightforward for the purposes of hydrostatic system control. However, as long as the temperature variation in the accumulator is kept low, the more directly measurable fluid/gas pressure can be used as an indicator of the SOC of the accumulator provided appropriate margins are considered [18, 22]. Therefore, the SOC can be estimated from the gas pressure as follows:

$$
SOC = \frac{p_g - p_l}{p_{\max} - p_l} \tag{2.8}
$$

where, p_l is the lower pressure limit of the accumulator corresponding to what is taken to be a zero SOC. The later should at least be equal to or greater than the pre-charge pressure of the high pressure (HP) accumulator for vehicle safety and accumulator reliability. Pictorially the above equation could be described as shown in Figure 2-8.

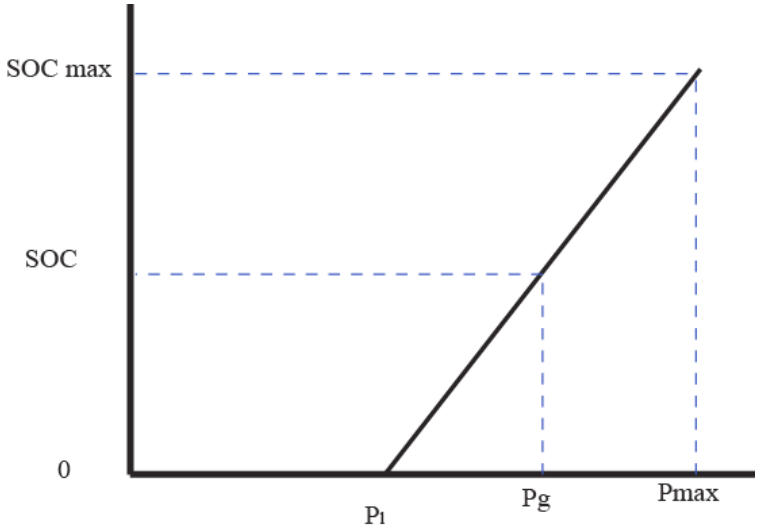

Figure 2-8 SOC estimation using gas pressure

2.2.2.3 Hydraulic Transmission Line Model

The hydraulic transmission lines carry high-pressure fluid throughout the system. They can be modeled with distributed or lumped parameter models depending on the required accuracy of the model. In the present application, the dynamic effects of the transmission lines (including compliance of the fluid and flexible hoses and the line inertances) are considered negligible since the frequency of interest is rather low (<10 Hz or so). This makes it possible to use a one-dimensional lumped parameter resistive model for the transmission lines instead of more elaborate dynamic and distributed parameter models [39, 40]. The causality of the hydraulic transmission line, shown in Figure 2-9, is

chosen in such a way that the inputs to the system are the upstream flow rate and the downstream pressure whereas the outputs of the model are the upstream pressure and the downstream flow rate

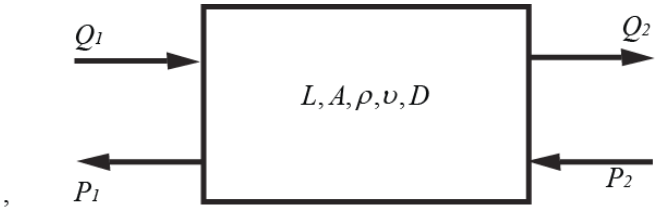

Figure 2-9 Causality of hydraulic transmission lines

The resistive pressure drop along transmission lines and fittings can be expressed mathematically as a function of the Reynolds number [36]:

$$\Delta p = p_1 - p_2 = f \frac{L\rho Q_a^2}{2D_0 A_p^{\ 2}} \tag{2.9}$$

where, L is the total effective length of the transmission line between two components (indexed *1*, and *2*), ρ as the fluid density, Q as the flow rate through the pipe/hose, D_0 is the internal diameter of the pipe, and A_p as the cross sectional area of the pipe. The friction coefficient f is given by:

$$f = \begin{cases} 64 / \mathrm{Re} & \mathrm{Re} \le 2000, \quad \text{laminar flow} \\ 0.332\,\mathrm{Re}^{-1/4} & 2000 < \mathrm{Re} < 10000, \quad \text{turbulant flow} \end{cases} \tag{2.10}$$

where Re is the Reynolds number and is defined by $\mathrm{Re} = \frac{4Q_a}{\pi D_0 \nu}$ where, ν is the kinematic viscosity of the fluid. Combining the above equations, the high pressure side of

the motor or pump, i.e., the motor inlet pressure and the pump discharge pressure are given by:

$$p_{p/m,p} = p_j + \text{sgn}(Q_a)\Delta p_f \quad \textbf{(2.11)}$$

The junction pressure P_j is related to the gas pressure P_g considering the accumulator flow rate through the inlet orifice.

$$p_j = p_g + \text{sgn}(Q_{acc})Q^2{}_{acc}K \quad \textbf{(2.12)}$$

where a constant $K = \frac{\rho}{(2(C_d A_{orifice})^2)}$ contains the orifice parameters: the discharge coefficient C_d and its area $A_{orifice.}$, and the density of the fluid.

2.2.2.4 Junction Model

A schematic of the model for a 3-port hydraulic junction is shown in Figure 2-10. Here the pressure assumed fixed by port 1. This pressure which is dictated by the accumulator gas pressure from Eq. (2.12) is passed without modification to the two other ports. To ensure compatibility with the causality of the model, Figure 2-4, the flow rate input at ports 2 and 3 are summed to compute a flow rate output at port 1.This is extracted from the power flow equation as follows (neglecting fluid storage or compressibility at the junction):

$$p_1Q_1 = p_2Q_2 + p_3Q_3 \quad \textbf{(2.13)}$$

$$p_1 = p_2 = p_3$$
$$Q_1 = Q_2 + Q_3 \quad \textbf{(2.14)}$$

In our case, p_i , $i=1,2,3$ stands for junction pressure ,p_j, Q_1 stands for junction flow (Q_j), Q_2 stands for pump flow (Q_p) and Q_3 stands for the total P/Ms flow rate ($\sum Q_{p/m}$).

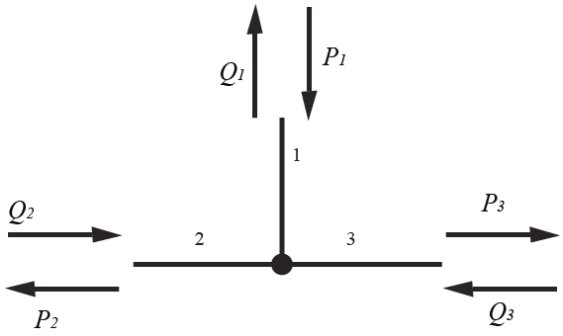

Figure 2-10 Three port hydraulic junction model

2.2.2.5 Total Volume Constraint

Finally, the constraint that has to be considered in this model is that the total volume of the oil in the hydrostatic powertrain remains constant at all times. i.e.:

$$V_{oil,total} = V_{oil,acc} + V_{oil,res} + V_{oil,pump} + V_{oil,P/M} + V_{oil,transline} = cons$$

2.2.3 Engine Model

The engine subsystem model takes the load torque (T_L) and the engine power (P_e) signals as an input from the pump and the supervisory controller, respectively, and gives the engine speed and the fuel consumption values as an output. See Figure 2-11.

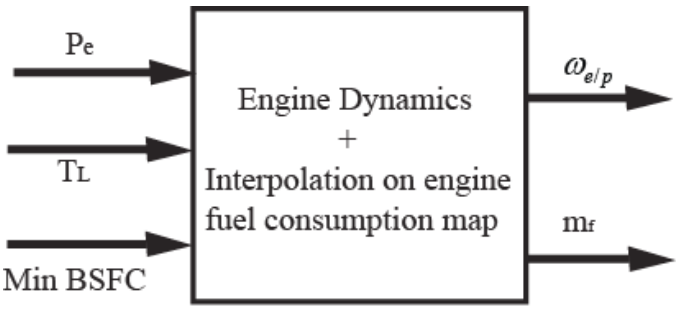

Figure 2-11 Engine sub model

The model of the engine subsystem is implemented as quasi-steady state lookup table from the fuel consumption map of the engine and incorporates the dynamics of the engine/pump (e/p) rotational inertia. It is first assumed that engine power (P_e) is determined by the power management strategy (described below) in the supervisory system controller. Given the engine power P_e, one can read, from the engine map, the desired engine torque T_e and desired engine speed ω_{e_des}, corresponding to the minimum BSFC (brake specific fuel consumption) line of the engine at that power level. The relevant lines are shown in Figure 2-12. By neglecting torque generation delays, it is assumed here that the actual engine torque matches the desired. The actual speed of the engine-pump ($\omega_{e/p}$), however, is determined from the engine-pump rotational dynamics given by the equation below:

$$T_e - T_L(x_p, \omega_p, \Delta p_p) = J_{eq.} * \frac{d\omega_{e/p}}{dt} \qquad \textbf{(2.15)}$$

where T_L is the load torque (pump torque) on the engine, and J_{eq} is the equivalent engine-pump rotational inertia.

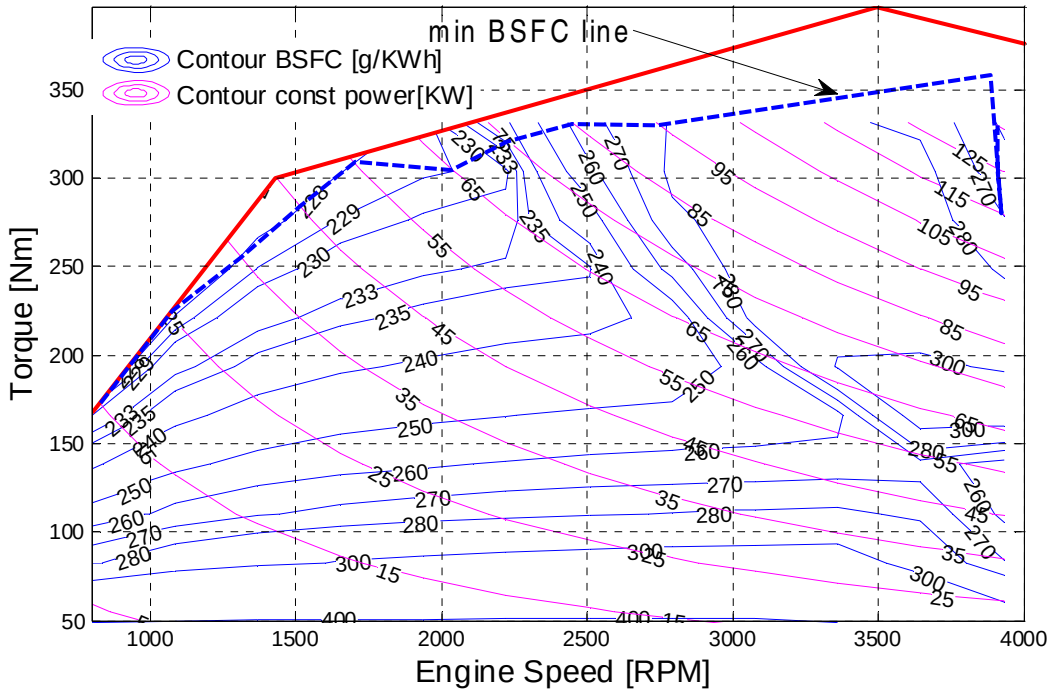

Figure 2-12 4.6 L Triton V-8 engine map with constant power and brake specific fuel consumption lines including the minimum BSFC line

The actual speed of the engine/pump from Eq. (2.15) is controlled via the displacement of the pump (through its displacement factor x_p) to track the desired engine speed, ω_{e_des}, which is selected based on the minimum BSFC speed of the engine at the current power level. A PI controller is used to minimize the speed error from this value:

$$x_p = K_p(\omega_{e\_des} - \omega_{e/p}) + K_i \int (\omega_{e\_des} - \omega_{e/p}) \cdot dt \qquad \textbf{(2.16)}$$

Here, k_p and k_i are the proportional and integral gains. Note that the displacement factor x_p influences the pump torque via Eq. (2.2) and eventually the engine speed via Eq.(2.15).

2.2.4 Longitudinal Vehicle Dynamics

For evaluating the longitudinal performance of the vehicle, the engine subsystem and the hydrostatic powertrain models described above are integrated with vehicle dynamics via the tire-wheel dynamics, whose free-body diagram is shown in Figure 2-13. By neglecting the longitudinal wheel slip of the tire, the tire-wheel dynamics can be described as:

$$T_w - F_x R_w = J_{weq} \frac{d\omega_w}{dt} \tag{2.17}$$

where, $J_{w\ eq}$ is the equivalent inertia of the motor and the wheel referred to the wheel, ω_w is the rotational speed of the wheel, T_w is the driving torque exerted at the wheel by the pump/motors, R_w is the radius of the wheel, and F_x is longitudinal tire force.

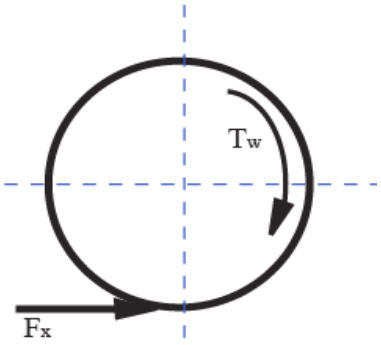

Figure 2-13 Wheel of the vehicle

The longitudinal tire force is related to the vehicle speed through the longitudinal equation of motion for the vehicle (Newton's 2nd Law):

$$F_x = \frac{m\frac{dV}{dt} + 1/2\rho C_d A V^2 + f_0 mg\cos(\theta) + mg\sin(\theta)}{n} \quad \textbf{(2.18)}$$

where, V is the speed of the vehicle, ρ density of the air, C_d drag coefficient, A is the frontal projected area of the vehicle, f_0 rolling resistance coefficient of the tire, g gravitational acceleration, θ is the road elevation and n is the number of motors actively engaging in driving the vehicle. In most of work involving powertrain energy use analysis, longitudinal wheel slip is considered negligible. The wheel speed is then related to vehicle speed through the no-slip condition:

$$\omega_w = \frac{V}{R_w}. \quad \textbf{(2.19)}$$

This assumption is not a necessary one when elaborate tire models are considered as for analysis of vehicle stability control with the present independent wheel drive system.

Plug in Eq. (2.18) and Eq. (2.19) in to Eq. (2.17), and rearrange it, the driving torque at the wheel is then giving by Eq. (2.20).

$$T_w = \frac{J_{weq}}{R_w}\frac{dV}{dt} + \left(\frac{m\frac{dV}{dt} + 1/2\rho C_d A V^2 + f_0 mg\cos(\theta) + mg\sin(\theta)}{n} \right) R_w \quad \textbf{(2.20)}$$

The bent-axis hydraulic motors are mechanically coupled to the wheels of the vehicle through a single gear ratio speed reduction unit, which results in the following equations for the torque ($T_{p/m}$) and the speed ($\omega_{p/m}$) of the pump/motor respectively.

$$T_{p/m} = \frac{T_w}{i_g}\eta_g^{\pm 1} \quad \textbf{(2.21)}$$

$$\omega_{p/m} = i_g \omega_w \quad \textbf{(2.22)}$$

Here, i_g stands for transmission gear ratio, η_g stands for the transmission efficiency with (-) superscript for motor (driving) mode and (+) superscript for pump (braking) mode.

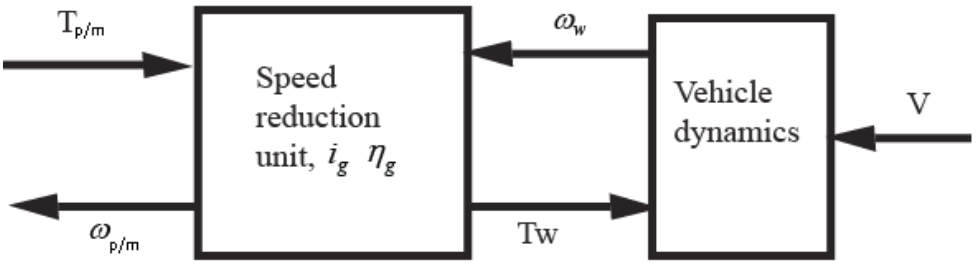

Figure 2-14 Causality of vehicle dynamics and speed reduction unit

2.2.5 Driver Model

A PI controller is tuned to mimic the driver as a vehicle speed controller and compute the motor displacement factor, $x_{p/m}$, using the error between the actual speed (V_{act}) and the desired speed (V) of the vehicle

$$x_{p/m} = K_p(V - V_{act}) + K_i \int (V - V_{act}) \cdot dt \quad \textbf{(2.23)}$$

This displacement factor at wheel-end P/M determines the P/M torque through Eq. (2.2).

CHAPTER THREE

3 RULE-BASED HYBRID POWER MANAGEMENT STRATEGY

In this Chapter, one of the hybrid power management strategies, rule-based, is described and presented in detail. The section also highlights the components of the hybrid power management strategies and the function of the overall top-level system supervisory control.

3.1 General Structure of Hybrid Power Management

The hybrid power management strategy is dictated by the top-level system supervisory control where in addition to power management strategy vie the engine and pump commands, vehicle stability control vie the individual wheel torque (displacement factor) command and supplementary friction brake activation command are determined to meet the energy efficiency, vehicle stability and safety objectives. If the vehicle needs to decelerate further while the torque available from the hydraulic system is not enough for braking or if the accumulator reaches maximum pressure, then the friction brakes need to be activated to bring the vehicle to the desired speed. In general, the supervisory controller (Figure 2-3) takes the vehicle states (longitudinal and lateral speeds, yaw rate, and rotational speed of individual wheels), the steering wheel angle and acceleration/braking signals, and the SOC of the accumulator as input commands from the sub-models of vehicle dynamics, driver and hydrostatic powertrain, respectively. It

then determines the individual wheel torques, the engine power and friction brake activation commands for the hydrostatic and vehicle dynamics subsystems.

A hybrid power management strategy is needed to determine the optimal split of the propulsion power demand between the two power sources (the engine-pump set or the accumulator) in such a way as to minimize fuel consumption and reduce emissions while maintaining (or improving) the drivability/performance (acceleration gradeability, and maximum speed) of the vehicle. The typical power management strategy can be considered to have a hierarchy of higher-level and lower-level control systems. The higher-level, supervisory type control system, determines the power demand from the engine to meet the driver's power request at any driving scenario while making sure that the accumulator state of charge (SOC) is maintained low enough to create conducive environment for effective energy regeneration during braking. The lower-level control systems, on the other hand, determine the engine operating points on the torque-speed map for optimum efficiency (near the minimum BSFC regime) at all power level determined by the higher-level control. The lower-level system may also include a speed regulator that attempts to bring the actual engine-pump speed to the desired engine speed.

In this thesis, three power management strategies are evaluated for the series hydraulic hybrid vehicle with independent wheel drives using the detail models presented in Chapter 2. The first strategy, which is detailed in this Chapter, is an experiential a rule-based strategy proposed by Kim and Filipi [22]. The second and third strategies are based on optimization. Global optimal power management strategy obtained through dynamic programming for a known drive cycle and a sub-optimal instantaneous consumption

minimization strategy are detailed in the next Chapter as a first application to series hydraulic hybrids.

3.2 Rule-Based Strategy

Simple and robust to implement, rule-based power management strategies, are based on rules set by the control engineer to split the power demand between the two power sources in such a way that these power sources are operating close to their high efficiency region. The rules depend on the values of the selected variables that could ultimately determined the power split. These variables include, but are not limited to, the power demand at the wheels, the driver's acceleration command, accumulator state of charge (SOC) and so forth [19].

The common type of rule-based power management strategy is a thermostatic SOC or "bang-bang" control scheme [19, 41]. In this type of strategy, the accumulator SOC is allowed to vary between upper and lower threshold values so that when the SOC reaches the upper limit the engine is turned off and the power request is entirely supplied by the accumulator alone. When the SOC reaches the lower limit, the engine is turned on and begins charging the accumulator with a predetermined power level set by the controller that runs the engine at its most efficient point.

The rule-based power management strategy taken in this thesis is adopted from [22]. It is a thermostatic SOC control in nature with some modifications to allow for continuous variable transmission (CVT) mode of the series hybrid powertrain at higher

power demands. Figure 3-1 shows a schematic of the power management strategy. Here, the SOC of the accumulator is the only variable used to dictate the engine power (P_e).

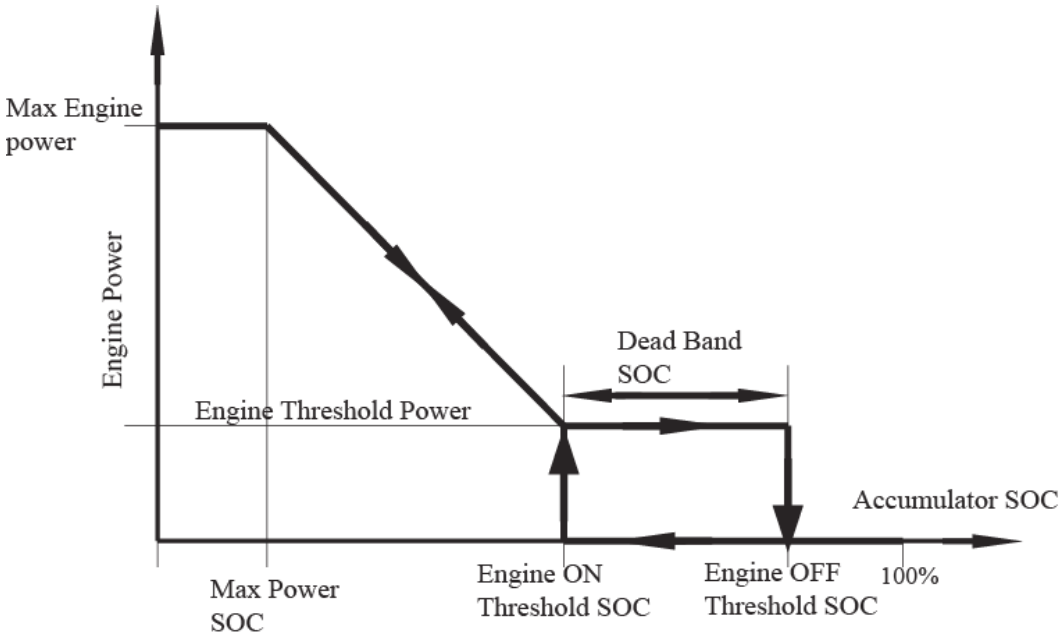

Figure 3-1 Schematic representation of engine power as a function of SOC

In this strategy, the engine power command (P_e) increases or decreases progressively based on the SOC of the accumulator. As long as the SOC is above the Engine-OFF threshold value, say 40%, the engine power command is set to zero, and the drive power is supplied entirely from the accumulator. When the SOC of the accumulator drops below the threshold value, the engine starts charging the accumulator and/or contributing to the drive power, while running at the predetermined threshold power command (say 45 kW, for this work). An SOC dead band of 10% or so is taken to alleviate frequent engine on-off cycling. If the power demand is such that it exceeds the engine threshold power and the SOC drops below the Engine-ON threshold SOC of the dead band (say 30%), the engine power command is progressively increased along the

minimum BSFC line on the torque-speed map of the engine. With further increase in propulsion power demand, the powertrain works in a hydrostatic continuously variable transmission (CVT) mode, with the engine operating at a maximum power trying to keep the SOC of the accumulator above a minimum (Max Power SOC, say 10%).

After the engine power is determined by this rule-based power management system, the engine operating points, i.e. the desired engine speed (ω_{e_des}) and torque (T_e) are extracted from the intersection of the constant power line and the minimum BSFC line on the engine map, as shown in Figure 2-12.

3.2.1 Verification of System Model with Rule-Based Strategy

3.2.1.1 Setting Component Specifications and Thresholds

The system model described in Chapter 2 and the power management strategy described above were implemented in Matlab/Simulink. The model was then used to select component sizes and control threshold parameters for the independent hydrostatic drive system proposed in Figure 2-1, with the objective of improving mileage and longitudinal performance for a mid-size truck. The analysis started with the stock engine for a Ford F-150 truck (4.6 L, V-8, 172kW SI engine) and considered that the upgraded powertrain with the independent drive should propel a larger truck with a GVW of 8000 lbs (about 20% heavier). In addition, the selection of the hydrostatic components was limited to stock components for which test data were available. The following components were obtained as the result of the iterative optimization and component

selection exercise: P/M displacement of 55 cm^3/rev; engine mounted pump displacement of 125 cm^3/rev and gear ratio between the P/M and the wheel of 4.00.

The size of the energy storage unit, i.e., the accumulator, plays a vital rule in fuel economy and performance improvement of the vehicle. With the other components specified as above, the size of the accumulator is considered for further system optimization. Using three standard accumulators (10, 15, and 20 gal) together with the aforementioned sets of component sizes, further fuel economy optimization and safety considerations led to the following sets of parameters for the accumulator and engine operating thresholds: Pre-charge pressure =13 MPa, Maximum pressure = 40 MPa, Engine-OFF SOC threshold = 40%, SOC dead band = 10%, threshold engine power =45 kW. A similar and more detailed analysis of component sizing, threshold parameter selection and optimization of the selected parameters for a series hydraulic hybrid vehicle can be found from [22]. These sets of component sizes and operating threshold parameters are used for the rest of the discussion unless otherwise specified.

3.2.1.2 System Performance with the Rule-Based Strategy

City Cycle

In this subsection, the results for the longitudinal performance of the system in the Federal Urban Driving Schedule (FUDS) are presented. Figure 3-2, Figure 3-3, and Figure 3-4 show some of the responses of the system for the first 400 seconds of the drive cycle for 4-wheel (4-motor) drive case. The accumulator and reservoir volumes were set at 20 gallons for the discussions that follow. Figure 3-2a, shows the actual and desired

vehicle speed response plots. The maximum speed error is 0.1 kph over the trip. Figure 3-2b shows the time history plots of the accumulator SOC and vehicle speed and Figure 3-2c shows the engine and accumulator power. For the first 27 seconds, the engine power is zero as the SOC is greater than the Engine-ON threshold SOC. At the 20^{th} sec, the vehicle starts to accelerate with the power delivered only by the accumulator (negative accumulator power is discharging), but starting at the 27^{th} sec up to around 115^{th} sec the engine was turning on and off keeping the SOC fluctuation between 30% and 40% dead-band. The first substantial braking event starts at the 115^{th} sec and charges the accumulator to around 70% and the engine is turned off. During the period when the vehicle is stationary, between 125^{th} and 163^{rd} sec, the accumulator pressure is maintained nearly constant. When the vehicle accelerates rapidly (190-205 sec), the SOC of the accumulator drops below the Engine-ON threshold SOC value, and therefore, the engine power increases progressively to overcome the increased power demand by the vehicle and to recharge the accumulator.

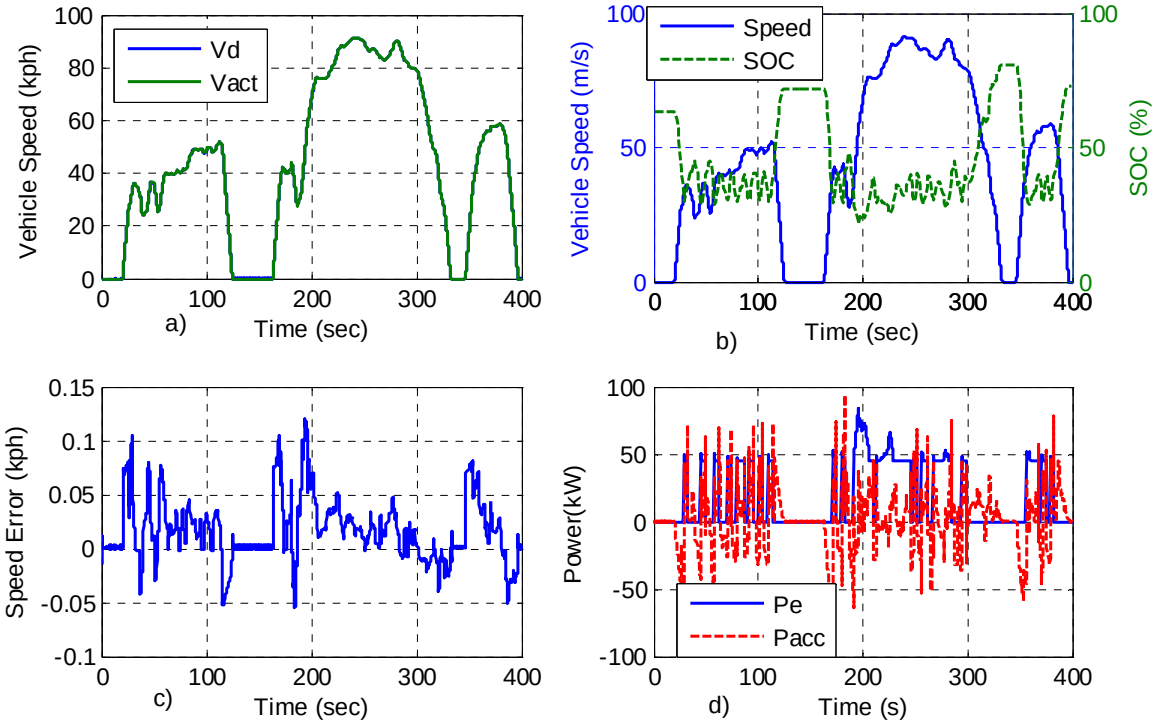

Figure 3-2 System responses of 4-motor drive for the first 400 sec of the FUDS cycle a) desired and actual vehicle speed time history plot, b) vehicle speed and accumulator SOC history, c) Vehicle speed error time history plot, d) Engine power (Pe) and accumulator power (Pacc) history plots

Figure 3-3b shows the time history plots of the gas pressures in the high-pressure (HP) and low-pressure (reservoir) accumulators. Figure 3-3c and Figure 3-3d show the corresponding torque and power output time history plots of one of the P/M units during the cycle. It can be observed that variation of the reservoir gas pressure (p_{res}) is negligible and remains low for the entire trip when compared with that of the HP accumulator gas pressure (p_g). This observation will allows us, in future model simplifications, to use a constant value of p_{res} for the reservoir without affecting the overall energy balance in the system. Figure 3-3c and Figure 3-3d show the torque and power output time history plots of a single P/M unit.

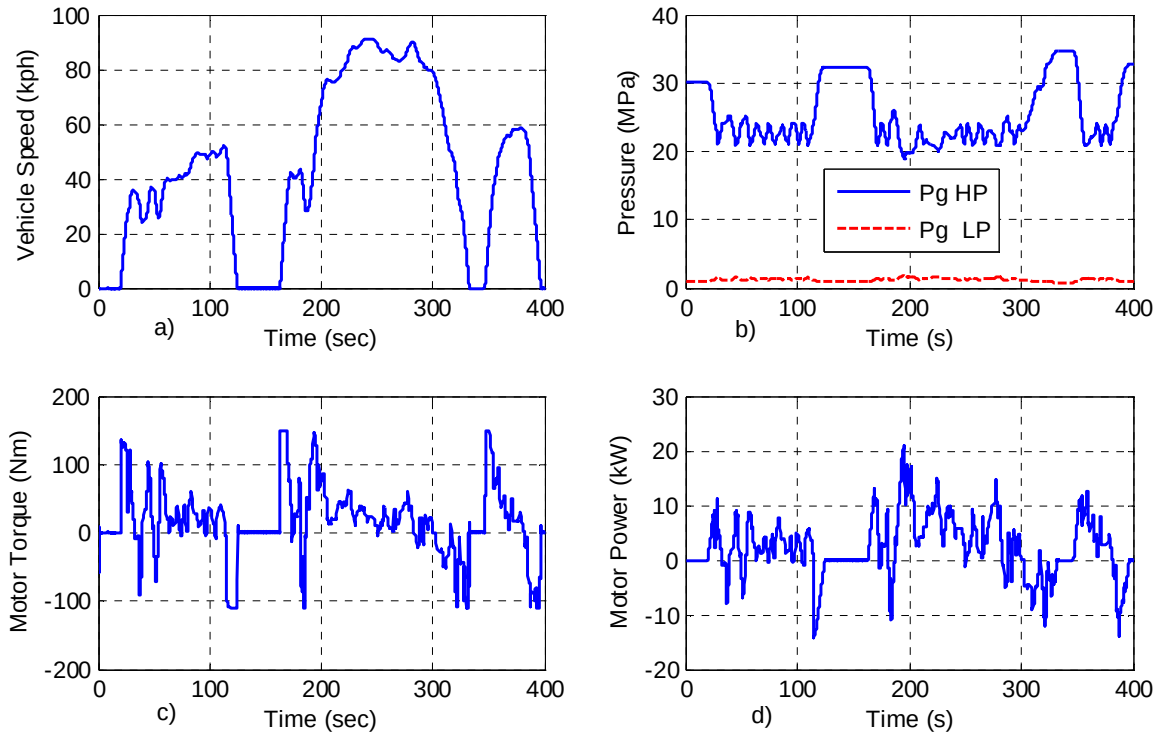

Figure 3-3 System responses of 4-motor drive for the first 400 sec of the FUDS cycle a) Speed profile, b) High pressure and low pressure accumulator pressure, c) P/M torque, d) P/M power

Figure 3-4a shows the engine operating points during the cycle superimposed on the torque-speed map of the engine. It can be seen how the operating points are concentrated on the minimum BSFC line for efficient engine operation. This plot demonstrates how the IC engine in a series hybrid vehicle can be controlled, independently of the road load, at its best efficiency points for fuel economy improvement and emission reduction. The motor displacement factor, $x_{p/m}$, is plotted on Figure 3-4c with negative value as motor (driving) mode and positive value as pump (braking) mode. Figure 3-4d depicts how the HP accumulator gas volume and oil volume varies with time for the driving cycle. Initially the accumulator volume was filled with equal volumes of the gas and oil. However, as the vehicle starts to accelerate, t=20 sec,

the gas volume increases (expansion) while the oil volume decreases, confirming the fact that the accumulator gives energy (losing its pressure) for propulsion. The first substantial braking event, t=115 sec, charges the accumulator and hence the volume of the oil increases while the volume of the gas decreases (compression) thereby storing energy as a form of pressure in the accumulator for later use.

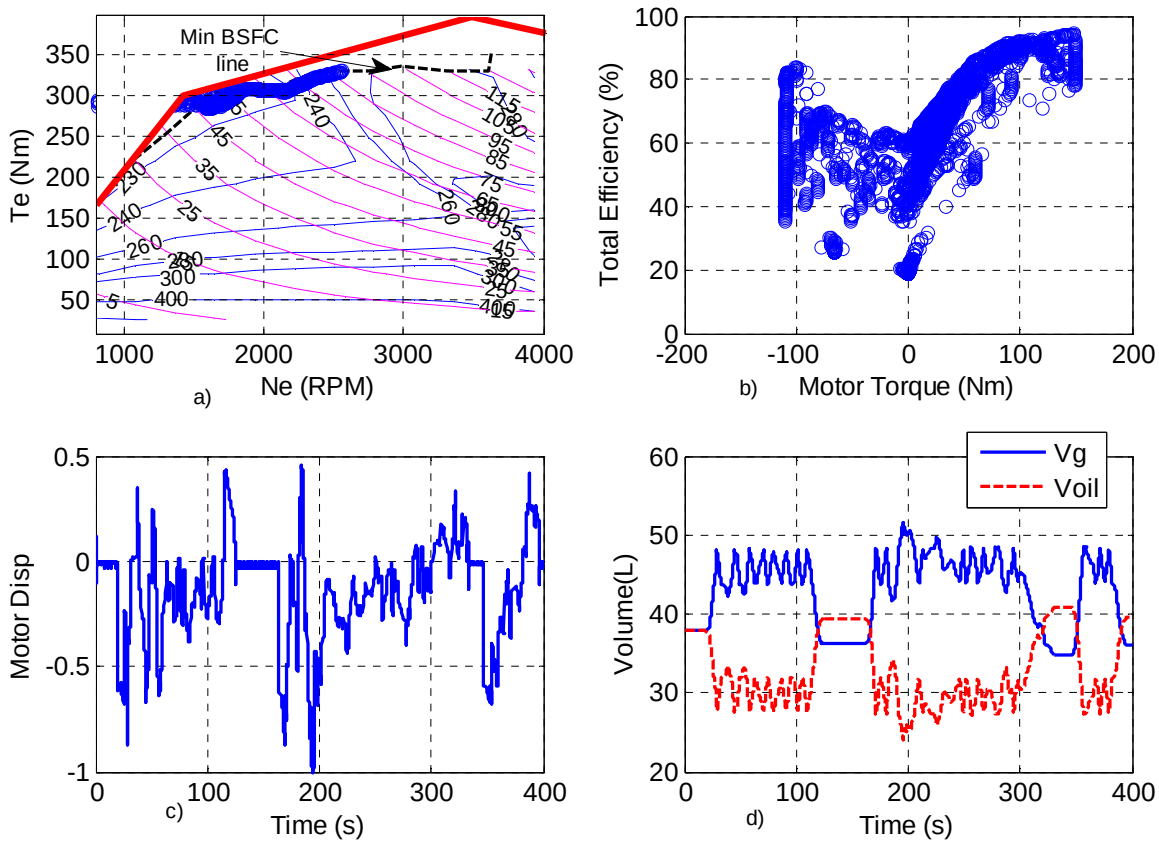

Figure 3-4 System responses of 4-motor drive for the first 400 sec of the FUDS cycle a) Engine operating points on its torque-speed map, b) Total efficiency and motor torque operating points of the P/M, c) Time history plots for displacement factor of the P/M, d) Gas volume and oil volume in the high-pressure accumulator

Highway Cycle

The results on the response/performance of the system on the highway drive cycle (the Highway Fuel Economy Test (HWFET)) are shown in Figure 3-5.

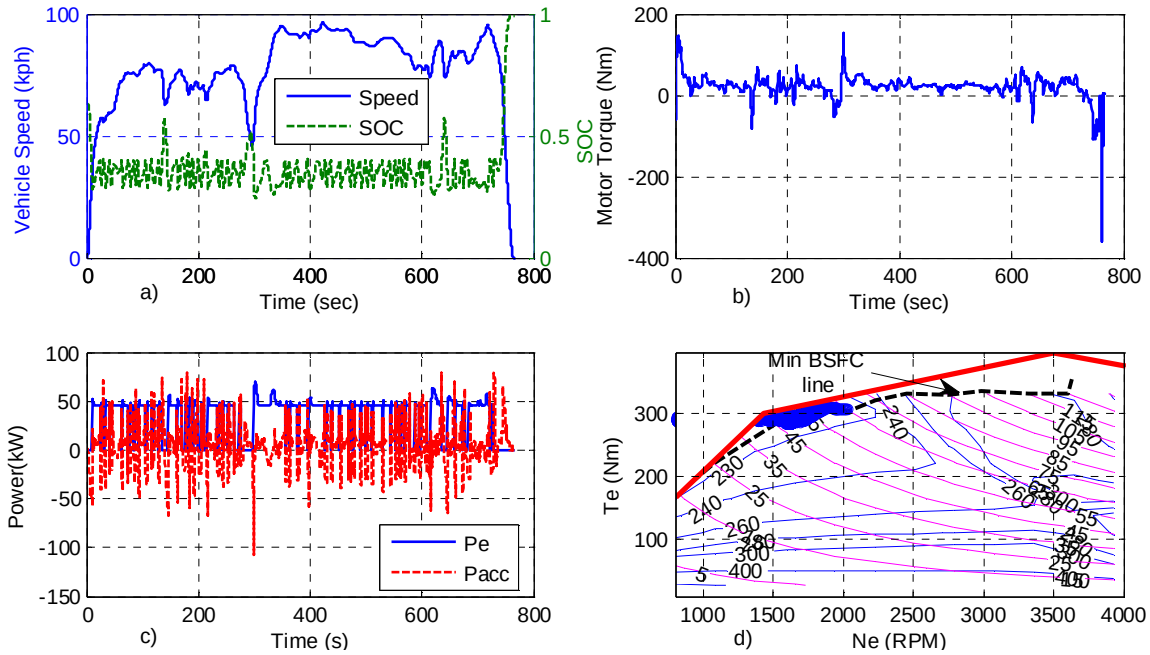

Figure 3-5 System response plots for HWFET cycle a) Vehicle speed and SOC time history plots, b) wheel-end P/M motor torque output, c) Engine power (P_e) and accumulator power (P_{acc}) plots, d) Engine operating points on the torque-speed map of the engine.

During the first 20 sec of the cycle, Figure 3-5a, the vehicle accelerates rapidly to reach to the top speed, leaving the accumulator SOC to drop suddenly within 10 secs (discharging mode). After 10 secs, the engine turns on and supplies power for both the wheels and the accumulator and keeps the SOC above the minimum threshold.

3.2.1.3 Comparisons in Fuel Economy Improvement over Conventional Drive System

A cursory look at the fuel economy results in Table 3-1 indicates the expected significant benefits from the hybridization, particularly in city driving where 32% fuel economy improvement is achieved over the conventional powertrain of the vehicle.

As the highway cycle is characterized by the absence of frequent stop-and-go motion, no substantial braking events exist for possible kinetic energy regeneration. As a result, the engine power is used as a main source to drive the vehicle while maintaining the SOC of the accumulator within the dead-band. This means there will be losses in multiple energy inter-conversions from engine-to-pump-to-motor-to-wheel. In addition, the low motor torque requirement at the wheels of the vehicle means the motors operate in part-load with poor efficiency. These factors make the overall system performance to be somewhat compromised and the fuel economy improvement is not as attractive as that obtained in the city cycle. However, the overall fuel economy on the HWFET is still better than that of the conventional drive because of the basic ability of the current system run the IC engine near its optimum efficiency (See Table 3-1).

Table 3-1 Fuel economy improvement comparison of independent hydrostatic wheel drive over the conventional truck

	Conventional Truck, Ford F-150, 4WD, V8, 4.6L, Automatic 4spd [US DOE, fueleconomy.gov] (MPG)	Independent Hydrostatic Wheel Drive (4-Motors) (% improvements)	Independent Hydrostatic Wheel Drive (2-Motors) (% improvement)
City Cycle (FUDS)	14	32	54
Highway Cycle (HWFET)	18	5	18.5

3.2.1.3.1 Comparison of 2-Motor vs. 4 Motor

Table 3-1 also includes results for a 2-motor drive at either the front or the rear axle. This is included to point out that the 2-motor drive does improve the fuel economy further with a 22% and 13% increments over that achieved with the 4-motor drive for city and highway cycles respectively. This can be explained by the fact that when the vehicle

is propelled by 2-motors, each of the motors takes up larger loads than the case with 4-motors (4WD), as shown in Figure 3-6b. Higher load (torque) is favorable for hydraulic machines as the efficiency of each machine increases with load. The benefits are illustrated further with Figure 3-7 which shows the cumulative effect through the percentage of total operating time spent within different total efficiency intervals during the FUDS city cycle. Clearly, the 2-motor drive system has the distribution shifted towards the higher efficiency values while the 4-motor drive has distribution tilted towards mediocre efficiency values. Due to the efficient operation of the P/M units, for 2-motor drive case, the recuperation process is more efficient and is characterized by the rise in the maximum available SOC of the accumulator from 80% to more than 95 % in comparison to 4-motor drive system, shown by Figure 3-6c. This increases the fuel economy by extending the period of operation of the accumulator before it completely discharges. However, the acceleration performance suffers when using the 2-motor drive as the two motors cannot supply as much torque as the 4 motors. Furthermore, 2-motor propulsion reduces the number of P/Ms that can act as wheel-end actuators for implementing vehicle stability control.

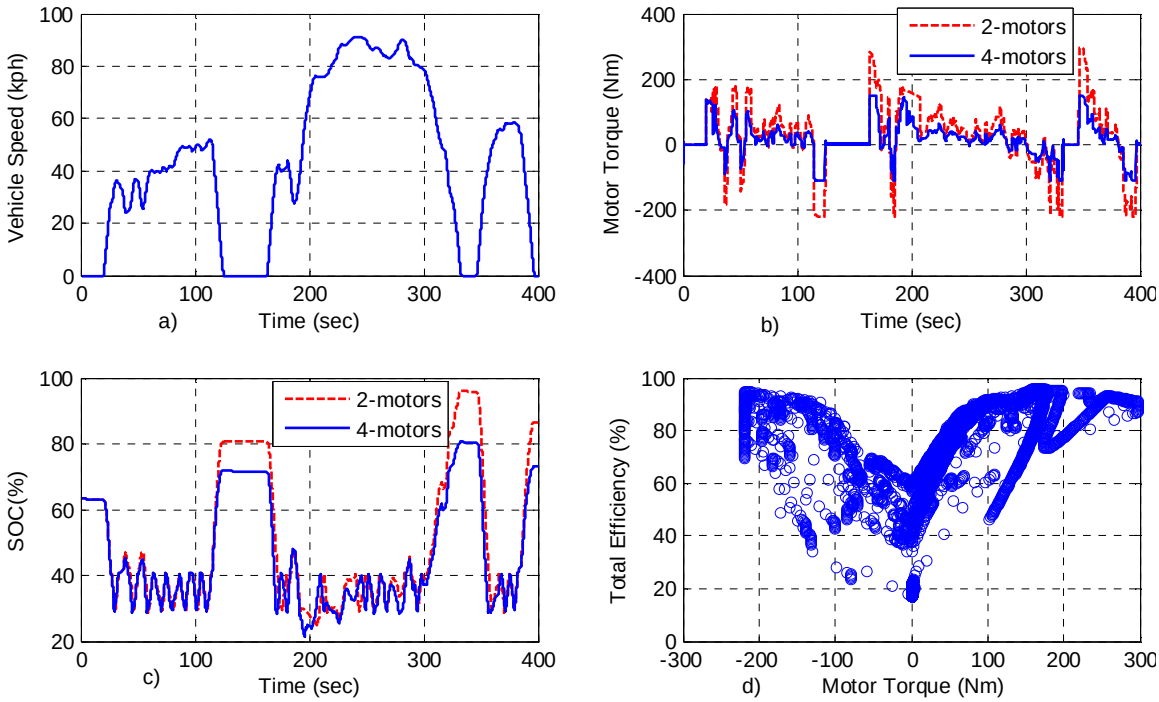

Figure 3-6 System comparison of 2-motor and 4-motor independent drive systems a) Speed profile of FUDS cycle for the first 400 sec, b) Wheel P/M torques for 2-motor and 4-motor independent drives, c) Accumulator SOC for 2-motor and 4-motor independent drives, d) Total efficiency and motor torque operating points of the P/M for 2-motor drive

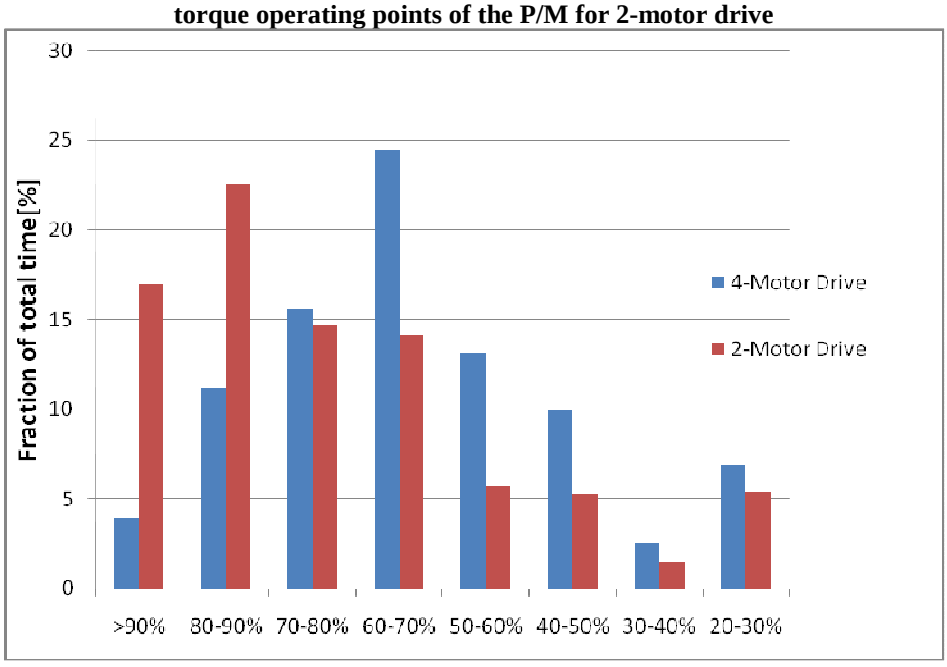

Figure 3-7 Comparison of cumulative effect on fraction of total operating time spent within the various total efficiency intervals for 2-motor and 4 motor independent drive systems for city cycle.

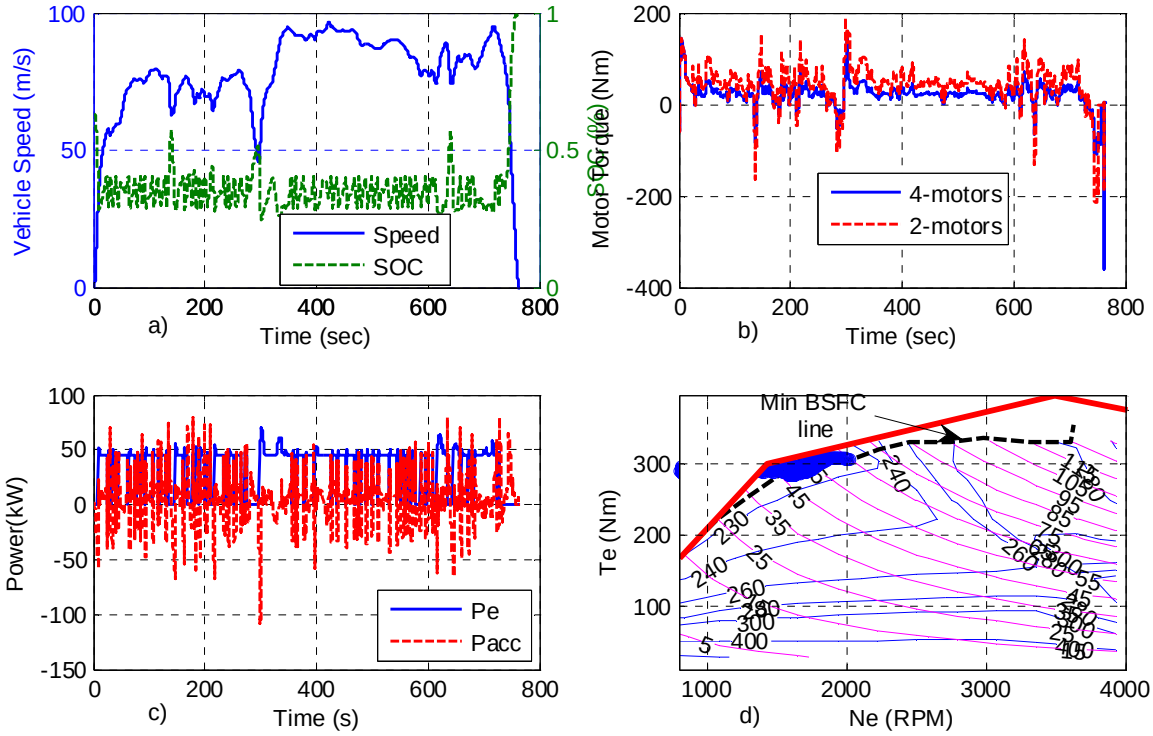

Figure 3-8 System response plots for HWFET cycle a) Vehicle speed and SOC time history plots, b) wheel P/M motor torque output for the 2-motors and 4-motors drive, c) Engine power (P_e) and accumulator power (P_{acc}) plots, d) engine operating points on the torque-speed map of the engine.

3.2.1.3.2 Effect of Accumulator Size

In this section, the system model and the rule-based strategy are used to analyze the effect of accumulator size on the performance of the vehicle. The simulation results are shown in Figure 3-9 and summarized in

Table 3-2. Looking at the fuel economy improvement for FUDS cycle with the 4-motor drive, a 15 gal accumulator gives better mileage than the 10 gal and 20 gal accumulators whereas the 10 gal accumulator gives more or less the same mileage as that of 20 gal accumulator as shown in Figure 3-10. The SOC of the 10 gal accumulator reaches 100% a number of times before the end of braking event as shown by Figure 3-9b and Figure 3-9c. During the periods of friction brake activation, some of the braking

energy, totaling around 0.3 MJ (6.3% of the total braking energy available at the wheels), is wasted as a form of heat at the friction brake pads in order to bring the vehicle to the desired speed. Losing this otherwise recoverable energy contributed for the reduction in fuel economy improvement with the 10 gal accumulator as compared to the 15 gal accumulator. The SOC of 20 gal accumulator never reaches 100% as depicted in Figure 3-9, and hence, it is able to recuperate all the braking energy available. However, the fuel economy is still less than that of a 15 gal accumulator. This is due to the fact that a vehicle equipped with the 20 gal accumulator has a 2.5% GVW increment over one equipped with the 15 gal accumulator, and a 5% increment over one with a 10 gal accumulator. This ultimately reduces the fuel economy due to increased load.

The other factor that contributes for the fuel economy improvement is the round trip efficiency of the accumulators for the same threshold operating points. For example, for the same pre charge and maximum pressure, the higher compression ratio of the smaller size accumulator improves its round trip efficiency compared to the larger accumulator. This can further be proved by Eq. (31).

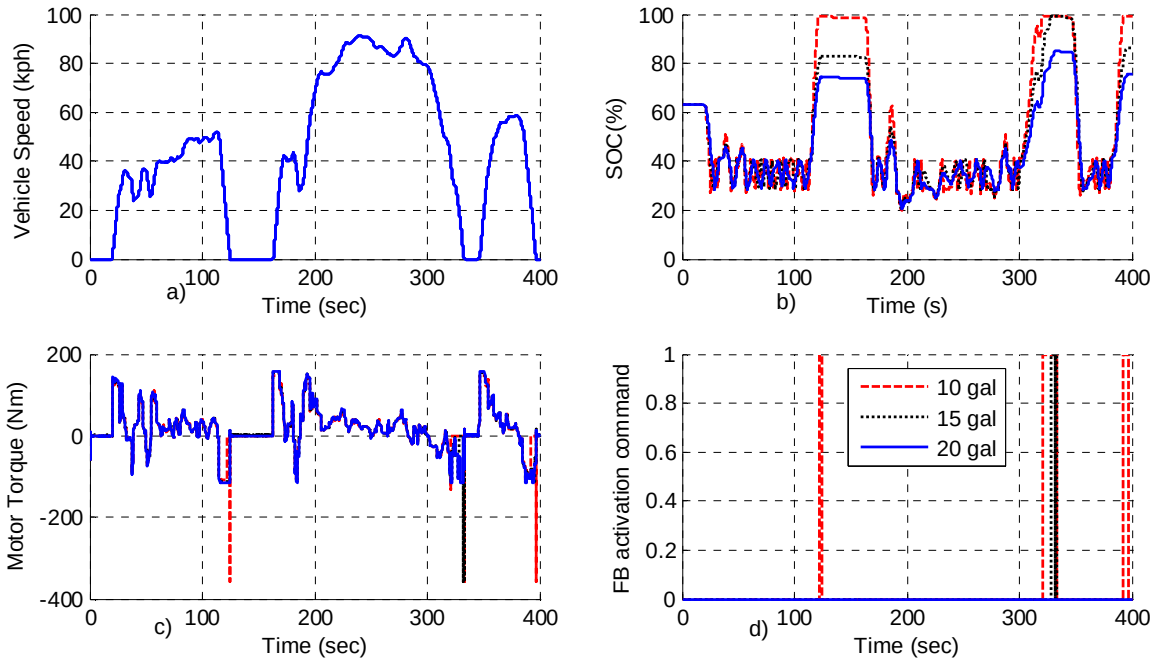

Figure 3-9 Effect of accumulator size on the performance of the vehicle a) portion of FUDS cycle for the first 400 sec, b) Comparison of SOC history, c) individual motor torque, d) Friction brake activation commands

The above discussion implies that there is a system level trade-off between frequent friction brake activation, roundtrip accumulator efficiency, and increased GVW. This explains why the intermediate size 15 gal accumulators give the best fuel economy improvement among the three sizes.

Table 3-2 Summary results of effect of accumulator size on the performance of the vehicle

	Accumulator volume (gallon)	City cycle (FUDS/UDDS)	High way cycle(HWFET)	0-50mph acc. time(s)
Conventional Truck, Ford F150, 4WD, V8, 4.6L, Automatic 4spd [US DOE, fueleconomy.gov] (MPG)	-	14	18	-
Independent Hydrostatic Wheel Drive (4 Motors, 4WD) (% improvements)	10	32	7.3	14.3
	15	34	6.3	14.2
	20	32	5	14.2
Independent Hydrostatic Wheel Drive (2Motors) (% improvement)	10	52	21	-
	15	55	20	-
	20	54	18.4	-

For the 2-motor drive case, in the FUDS cycle, the 15 gal accumulator gives a better mileage than the 10 gal and 20 gal accumulators as shown in Figure 3-11. However, this time, the 20 gal accumulator gives better fuel economy than the 10 gal accumulator as the impact of the energy loss in the brake friction pads (totaling to 0.49 MJ) with the smaller accumulator far exceeds the impact of the increase in the GVW with the larger accumulator. For the HWFET cycle, where frequent stop-and-go motion is not prominent, the fuel economy improvement with the 10 gal accumulator is better than that with the 15 gal accumulator. Similarly, fuel economy improvement with the 15 gal accumulator is better than that with the 20 gal for both the 4-motor and 2-motor drive systems. This is attributed primarily to the lower GVW with the lower accumulator size.

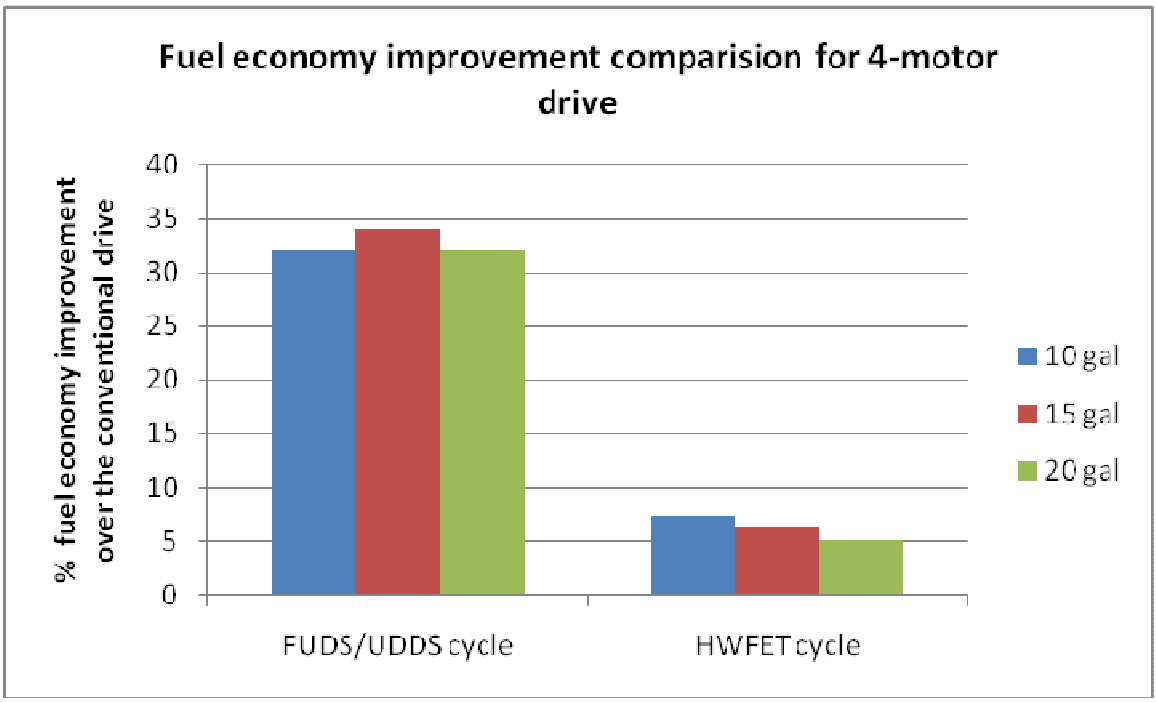

Figure 3-10 Effect of accumulator size on the performance of the vehicle for 4-motor drive system

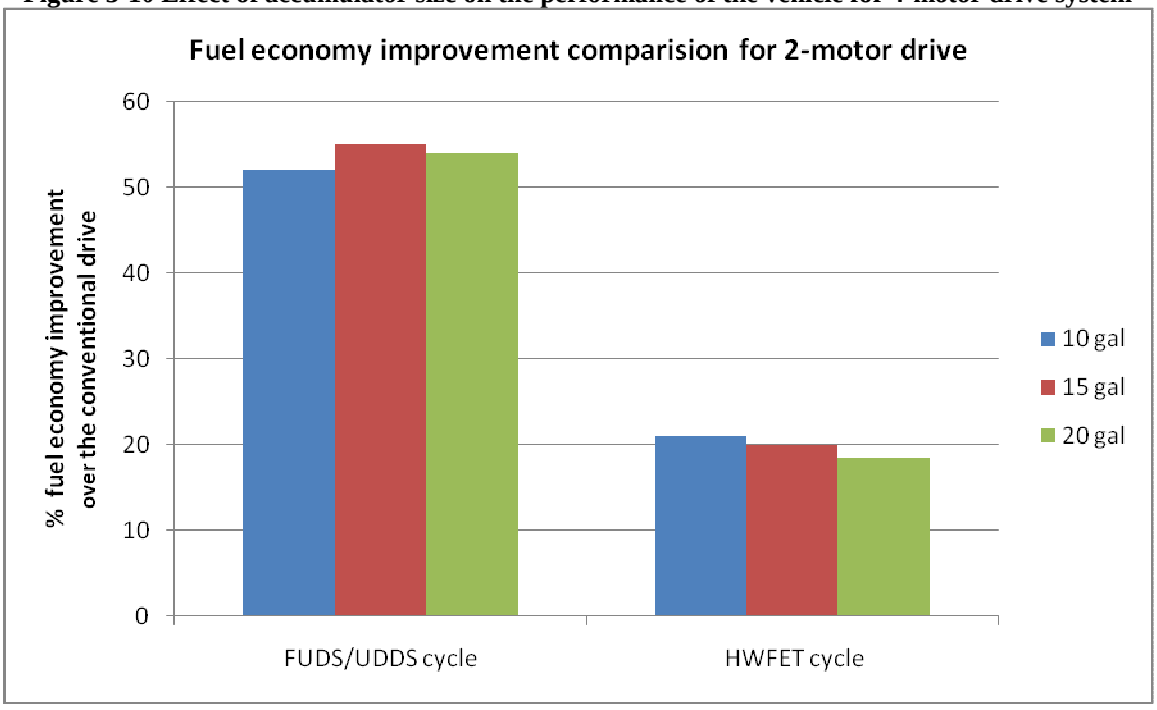

Figure 3-11 Effect of accumulator size on the performance of the vehicle for 2-motor drive system

The acceleration performance of the vehicle for different accumulator sizes is displayed on the last column of

Table 3-2. It shows that accumulator size has almost no impact on the acceleration performance. This is because the acceleration test is characterized by high power demand for short period of time (without breaking) as a result accumulator's effect is negligible as it delivers its energy immediately while the remaining power demand is supplied by the engine-pump alone until the end of the test. The acceleration performance could be further improved with an increased Engine-ON threshold SOC value. This is because, the accumulator pressure determines the junction pressure and hence the pressure available at the wheel-end P/Ms thereby higher threshold pressure means higher torque available at the wheels. But this is possible only at the expense of fuel economy improvement.

CHAPTER FOUR

4 OPTIMAL POWER MANAGEMENT STRATEGIES

In this Chapter, two optimization-based power management strategies will presented and applied to the hydrostatic (series hydraulic hybrid) powertrain described in Chapter 2. The rule-based power management strategy described in the preceding Chapter is not necessarily optimal. This is because of the following:

- Running the engine along its minimum BSFC line for each engine power demand doesn't consider overall system efficiency, rather considers only component efficiency (IC engine in this case). For example, the system efficiency of charging the accumulator from the engine-pump set depends on the efficiency of the engine, the pump, and the accumulator as well.
- It doesn't consider the nonlinear and dynamic nature of the system. As a result of this nature of the system, the threshold parameters giving better fuel economy result in one driving schedule may result inferior fuel economy result in another driving schedule.
- For a given or known drive schedule, it is possible, for example, that it is not best to fully charge the accumulator before the end of a hard braking events (See Figure 3-9). This may lead to lost opportunities in recovering more energy in the same or subsequent braking events. Such scenarios are not taken into account with the rule-based strategy.

Such limitations highlight the inadequacies of the rule-based power management strategy and are the impetus behind the need to seek and formulate optimal power management strategies.

4.1 Global or Trip Optimal Power Management

A globally optimal power management strategy determines the allocation of power demand between the on-board sources that gives the minimum integral fuel consumption over the whole duration of the trip or drive cycle. Generally, such a globally optimal solution requires or assumes that the load profile of the trip (or the drive cycle and road grade) is known ahead of time. In the present work, the globally optimal allocation or power split between the accumulator and the engine-pump are determined using dynamic programming.

Dynamic programming (DP) is a numerical technique for finding a sequence of time-varying state feedback control laws so that a cost function (e.g. total fuel consumption) is minimized over a priori known stages (drive profile). It works based on the principle of optimality proposed by Bellman [42, 43]. DP simplifies a complicated problem by breaking it down into simpler sub-problems and re-combining them in a recursive manner to arrive at a global solution. For a given dynamic system and cost function to be optimized (maximized or minimized), at each discrete time (stage), DP can search through all feasible discrete control inputs for all state grid points to generate global optimal solution with an accuracy of discretization interval The advantage of DP is

its ability to handle non-linear systems and constraints while generating the optimal control law.

In this thesis, the objective of the algorithm is to search the trajectories of the control signals, *u(k)*, including engine command (P_e and T_e) and pump command (x_p) to minimize the total fuel use over the driving schedule. Pollutant emissions are not considered in this work. Mathematically, the cost function can be stated as,

$$\min J = \min_{u(k)} \left(\sum_{k=0}^{N-1} m_f(u(k), y(k)) + h(SOC(N)) \right) \quad \textbf{(4.1)}$$

where m_f is the fuel use over the time segment, u and y are the vectors of control and state variables, N is the total driving cycle length under consideration and $h(SOC(N))$ is a penalty function that penalizes the deviation of the final SOC value from the initial SOC value if it is desired to maintain a charge-sustaining mode. In our case, a hard constraint is assumed where the final SOC is equal to the initial SOC. i.e. $SOC(N) = SOC(0)$ [44], as a result the net energy stored in the accumulator is zero thereby comparison of the hybrid powertrain with the conventional drivetrain can be made.

The detail hydrostatic powertrain-vehicle dynamics model, presented in Chapter 2 is not suitable for dynamic programming analysis due to its high computational burden. Therefore, a simplified but sufficiently detailed vehicle model that captures the basic behavior of the major components is needed. Figure 4-1 shows one such the simplified hydrostatic powertrain model developed in this work. It shows the power flow interaction between each component and the associated efficiencies that have been considered in the formulations of the DP algorithm. The engine-pump, the wheel-end P/M and the

accumulator are assumed to be directly connected at the junction with no pressure drop along the transmission lines. The pressure variation in the reservoir is very low and barely affects the overall equation of the system if it is taken as a constant. This was demonstrated through the results in Figure 3-3b. When the engine-pump speed dynamics is neglected, as it is fast compared to the dynamics the accumulator SOC, the only state variable that needs to be considered becomes the accumulator SOC.

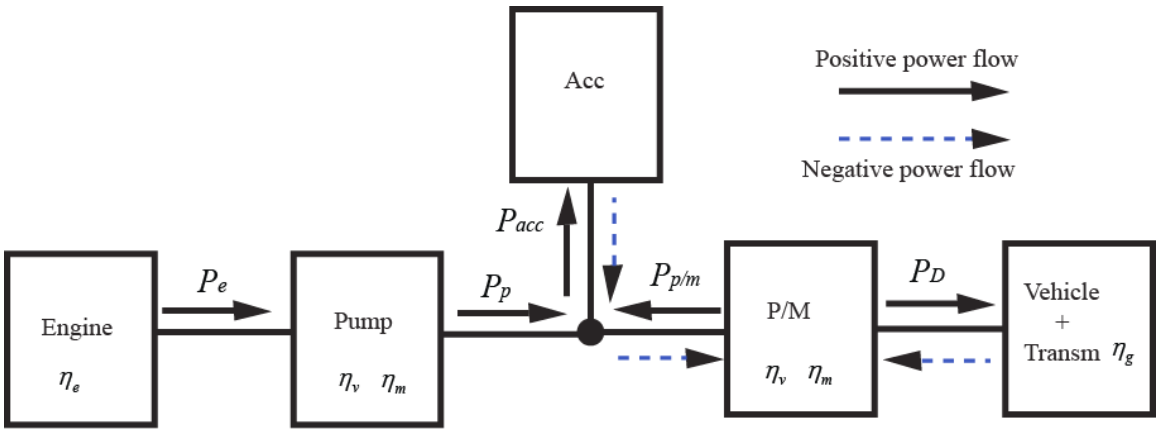

Figure 4-1 Simplified hydrostatic powertrain model for DP algorithm

Summing up the power at the junction, the power flow equation can be written as,

$$P_{acc} = P_p + P_{p/m} \tag{4.2}$$

where P_{acc} is power from/into the accumulator, P_p is the power from the engine-pump, and $P_{p/m}$ is the power from/into the P/M. Form Eq. (2.7), the dynamics of the accumulator SOC can be simplified as,

$$\frac{dSOC}{dt} = \frac{n \cdot Q_{p/m} + Q_p}{\mathrm{V}} \tag{4.3}$$

where the flow rate, $Q_{p/m}$, is taken to be the same for all the P/M units, n is the number of motors actively engaged in driving/breaking event and V is the total volume of the accumulator. The power flow in/out from the P/M units is given by the product of flow rate and pressure difference across the units. That is:

$$P_{p/m} = n \cdot Q_{p/m} \Delta p_{p/m} \tag{4.4}$$

Similarly, the power output of the pump is described as:

$$P_p = \Delta p_p Q_p \tag{4.5}$$

with the differential pressure given by:

$$\Delta p_{p/m} = \Delta p_p = \Delta p \tag{4.6}$$

Solving for the flow rate equations in terms of the power flow and Δp across the pump or the P/M from Eq. (4.4) and Eq. (4.5) and plugging it in Eq. (4.3), the SOC dynamics can be described as:

$$\left(\frac{dSOC}{dt}\right) = \frac{P_{p/m} + P_p}{\Delta p \cdot \mathrm{V}} = \frac{P_{acc}}{\Delta p \cdot \mathrm{V}} \tag{4.7}$$

Therefore, the power flow to/from the accumulator at each instant of time is given by:

$$P_{acc} = \left(\frac{dSOC}{dt}\right) \cdot \Delta p \cdot \mathrm{V} \tag{4.8}$$

The pressure difference across the pump and the P/M is given by:

$$\Delta p = p_g - p_{res} \tag{4.9}$$

Solving for p_g from Eq. (2.8) as a function of SOC and plugging it in to Eq. (4.9), Δp is given as:

$$\Delta p = SOC\left[p_{\max} - p_l\right] + p_l - p_{res} \tag{4.10}$$

The power demand, P_D, at the wheels of the vehicle required to follow the prescribed velocity profile on flat road is computed as:

$$P_D = \left(m\frac{dV}{dt} + \frac{\rho C_d A V^2}{2} + f_0 mg \right) \cdot V \tag{4.11}$$

The P/M power request, $P_{p/m}$, during driving and/or braking is then given by:

$$\begin{aligned} P_{p/m} &= \frac{P_D \cdot \eta_g^{\pm 1}}{n} \\ &= \frac{\left(m\frac{dV}{dt} + \frac{\rho C_d A V^2}{2} + f_0 mg \right) \cdot V . \eta_g^{\pm 1}}{n} \end{aligned} \tag{4.12}$$

For DP algorithm Eq. (4.8), (4.10) and (4.12) are discretized in Δt=1 second interval and rewritten as,

$$P_{acc}(k) = \left(\frac{SOC(k+1) - SOC(k)}{\Delta t} \right) \cdot \Delta p(k) \cdot \mathrm{V} \tag{4.13}$$

$$\Delta p(k) = SOC(k)\left[p_{\max} - p_l\right] + p_l - p_{res} \tag{4.14}$$

$$P_{p/m}(k)=\frac{\left(m\frac{V(k+1)-V(k)}{\Delta t}+\frac{\rho C_d A V^2(k)}{2}+f_0 mg\right)\cdot V(k)\cdot \eta_g^{\pm 1}}{n} \tag{4.15}$$

After rearranging Eq. (2.20) and (2.21), the P/M torque request is calculated, and discretized as,

$$T_{p/m}(k)=\left[\left(\frac{V(k+1)-V(k)}{\Delta t}\right)\cdot\left(\frac{n\cdot J_{weq}}{R^2{}_w}+m\right)+\frac{1}{2}\rho C_d A V^2(k)+f_0 mg\right]\frac{R_w \eta_g^{\pm 1}}{n i_g} \tag{4.16}$$

where (+) sign on the superscript stands for pump mode and the (-) sign stands for motor mode.

The P/M speed used to follow the given profile is calculated as:

$$\omega_{p/m}(k)=\frac{i_g V(k)}{R_w} \tag{4.17}$$

Since the engine-pump speed dynamics are neglected, Eq. (2.15) reduces to:

$$T_e=T_L(x_p,\omega_p,\Delta p_p) \tag{4.18}$$

For a given driving cycle, the P/M torque, $T_{p/m}$, and speed, $\omega_{p/m}$, required to follow the speed profile can be found from Eq. (4.16) and Eq. (4.17) at each time stage (time grid point). For each SOC grid points, as shown in Figure 4-2, the corresponding P_{acc} and Δp across the pump and P/M unit are found using Eq. (4.13) and Eq. (4.14), respectively. Then, the P/M displacement ($x_{p/m}$) can be chosen to produce the desired motor torques necessary for following the given speed profile. For a known P/M torque, speed, and displacement, $x_{p/m}$, and the knowledge of Δp, the efficiency of the P/M unit

can be extracted using 3-D interpolation from the efficiency map. Knowing the efficiency values, the power input (driving)/output (braking) of the P/M can be found by dividing/multiplying the motor power request according to Eq. (4.15).

For a known accumulator and P/M power values, the pump output power can be computed with Eq. (4.2), and is then known for each SOC grid points. To simplify the interpolations in the engine fuel consumption map and the pump efficiency map, the speed of the engine can be discretized in to a number of points. Corresponding to each engine speed grid point, the pump displacement can also be discretized and implemented as a vector for efficient computation in MATLAB. For known Δp, $\omega_{e/p}$ and x_p of the pump, one can then interpolate for the total efficiency η_t of the pump in its efficiency map. Then, the engine power, P_e, is found by dividing the pump power, P_p, with the total efficiency of the pump. This is comparable to the maximum engine power imposed by the constraint at that engine speed (see Eq. (4.19) below). If it doesn't violate the constraint, it will be selected. Otherwise, it should be modified to comply with the constraint.

After the engine power is computed, the engine torque is then computed from the relationship $T_e = \frac{P_e}{\omega_{e/p}}$. Finally, the engine torque and the engine-pump speed are used to interpolate the mass flow rate from 2D fuel consumption look up table and plugged into Eq. (4.1). By moving through all the possible points of the engine speed at a fixed SOC grid point, the minimum fuel mass will be determined and stored as a cost function.

The above calculation procedure is executed starting form the last stage of the driving cycle and is repeated at each stage advancing towards the first stage. Figure 4-2 shows a schematic of the whole process. At each stage, the algorithm computes and assigns the minimum cost and associated control inputs to each state grid points and then proceeds to the previous stage. This is repeated backwards in time until the whole drive cycle is covered. Along the way, the time-varying state feedback control inputs corresponding to each state grid points are found and stored.

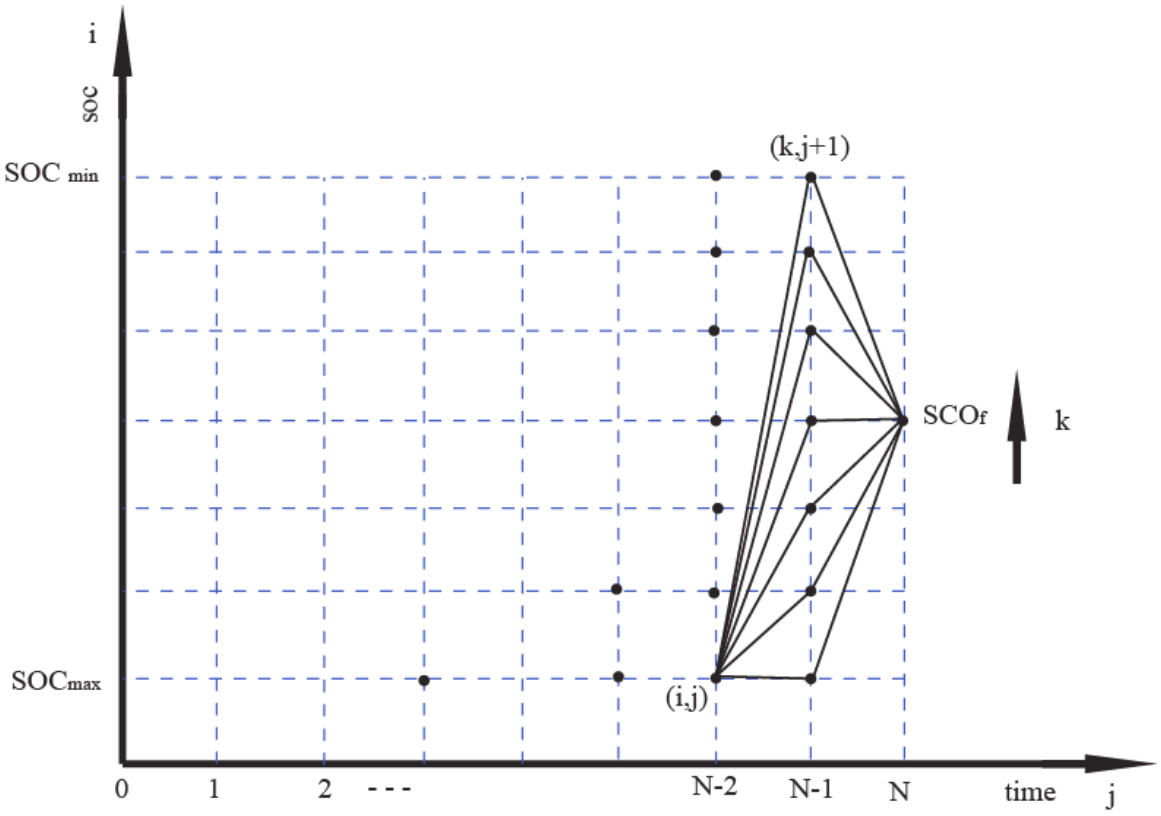

Figure 4-2 SOC grid points at each stage used for global optimization process

To ensure that the system operates with in physical limits for safety, the following physical constraints on the state and control inputs are taken in to consideration during the optimization process. A large penalty is assigned on the cost function for those signals that violates the constraints.

$$\begin{aligned} &\omega_{eng,\min} \le \omega_{eng}(k) \le \omega_{eng,\max} \\ &P_{eng,\min}(\omega_{eng}) \le P_{eng}(k) \le P_{eng,\max}(\omega_{eng}) \\ &SOC_{\min} \le SOC(k) \le SOC_{\max} \\ &0 \le x_p(k) \le 1 \\ &-1 \le x_{p/m}(k) \le 1 \end{aligned} \quad \textbf{(4.19)}$$

When the vehicle comes to a full stop, the engine could be turned off for maximum fuel economy improvement or it can idle with no engine-shutdown. These two sets of engine conditions have been considered for this algorithm.

The control and the state variables are discretized in such a way as to obtain a balance between decreasing the computation time requirement and increasing the accuracy of the result. To this end, the accumulator gas pressure is quantized in 2-bar intervals between 16 MPa and 40 MPa. This corresponds to 120 quantized bins for accumulator SOC each with intervals of 0.75%. The engine speed is divided in 100 rpm intervals and constrained between 800 to 3000 rpm. The engine side pump displacement factor is discretized in increments of 0.1 between 0 and 1.

4.1.1 Demonstration of DP Algorithm for a Simple Cycle

The DP algorithm presented in the previous section was implemented for the vehicle with independent 4-motor hydrostatic drive for city and highway drive cycles.

Simulations were then conducted to evaluate the use of different accumulator sizes in the system as well as to see the effect of different engine idling conditions.

To demonstrate the basic workings of the dynamic programming algorithm, the following simple driving cycle is chosen for discussion and to gain some useful insights into the optimal behavior for maximum fuel economy. This driving cycle is made of UN/ECE Elementary Urban Cycle part 1 with some modifications to include low, moderate, and high acceleration and braking events as well as cruising at low, moderate and high constant speeds, as shown in Figure 4-3. The results of the proposed algorithm for this driving cycle are summarized in Figure 4-4 and Figure 4-5. The engine power (P_e), engine torque (T_e) and pump displacement (x_p) plots show the optimal control trajectories to achieve minimum fuel consumption. For the first 10 sec, the vehicle is stationary (A-B) while the engine power is used to charge the accumulator as shown by both the rise in the SOC of the accumulator, Figure 4-4a, and the positive accumulator power (charging), Figure 4-4b, This is to bring the system pressure to the desired level where required wheel torque can be delivered. During the subsequent low-power acceleration phase (B-C), the accumulator delivers its power (negative accumulator power, discharging) for propulsion with small assist power from the engine side. When the SOC of the accumulator gets low, the engine power increases to keep the pressure in the accumulator high as well as to deliver the power to the wheels, characterized by high T_e, x_p and ω_e. During the low speed cruising at 30 kph, phase (C-D), the engine is delivering power for both the wheels and the accumulator so as to increase the pressure of the accumulator to bring the system pressure to a desired level for the braking event

and recovery opportunity ahead. When the first braking event happens (D-E), the accumulator pressure increases (positive accumulator power, charging) as it stores braking energy while the engine power output decreases, shown by low T_e , ω_e and x_p, Figure 4-4, where the engine is operating close to its least fuel consumption point for the given power requirement.

Engine shutdown is not considered in this case. Therefore, during segment E-F, when vehicle has stopped, engine is charging the accumulator by a small power to raise the pressure to close to higher value (30 MPa) in anticipation of the coming acceleration ahead (F-G). During segment F-G both the engine and the accumulator are driving the vehicle to overcome the large driving power requirement, as shown by large negative power of the accumulator and large power of the engine. The high speed cruising segment G-H power demand is just enough to be supplied by the engine alone while the pressure in the accumulator remains constant as no power is flowing to/from the accumulator.

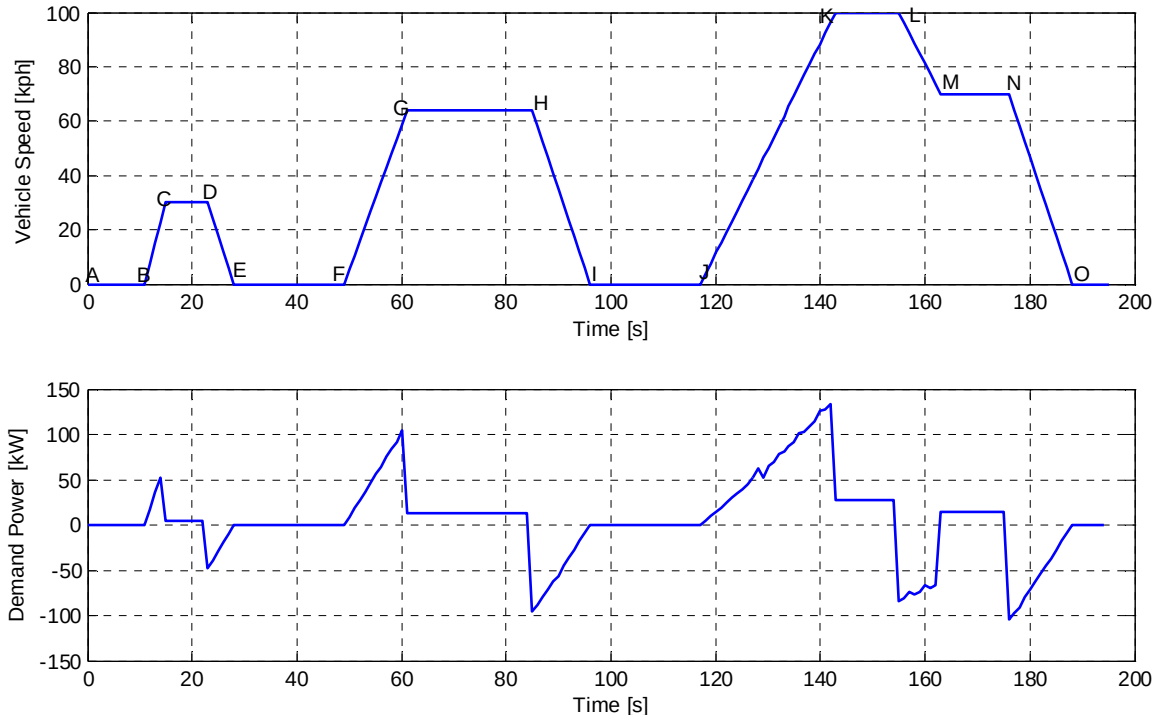

Figure 4-3 A modified Elementary urban driving cycle part 1 used for the purpose of DP discussion

Engine power is minimal during braking and standstill that follows (H-I-J) while the accumulator harvests braking energy. During segment I-J, when vehicle has stopped, engine is charging the accumulator to raise the pressure to close to its maximum allowed value (39 MPa) in anticipation of the hard acceleration ahead (J-K).

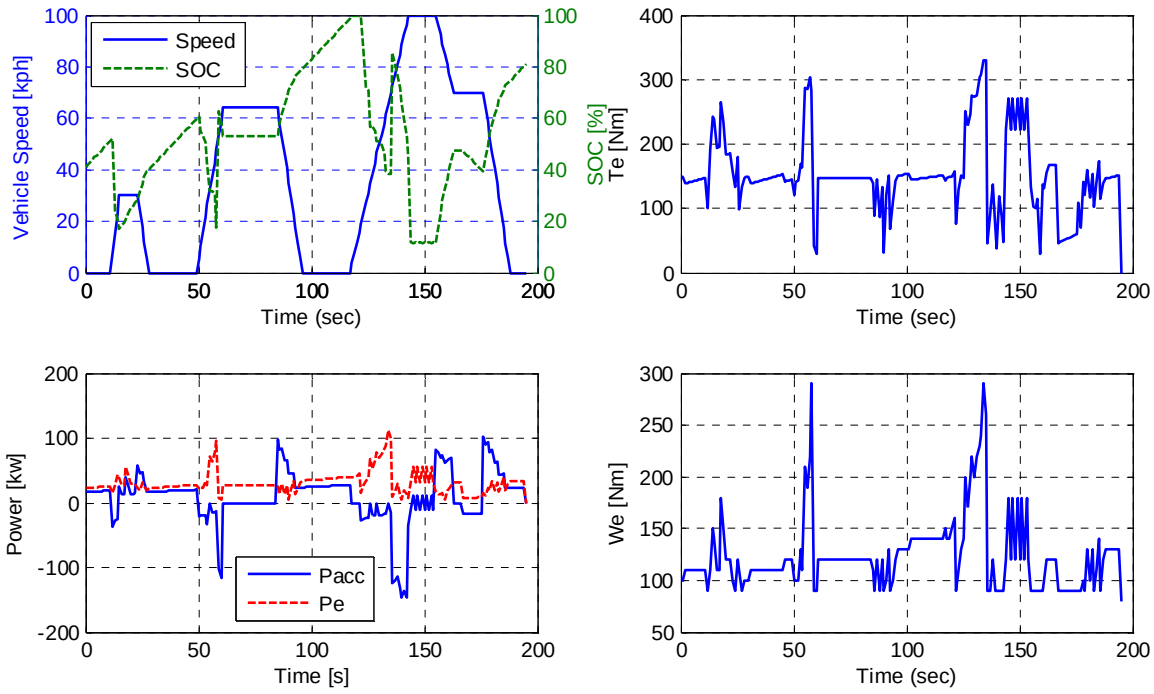

Figure 4-4 DP result plots for modified elementary urban driving cycle a) Vehicle speed and SOC time history plots, b) Engine torque command history, c) Accumulator and Engine power command history, d) Engine speed command history

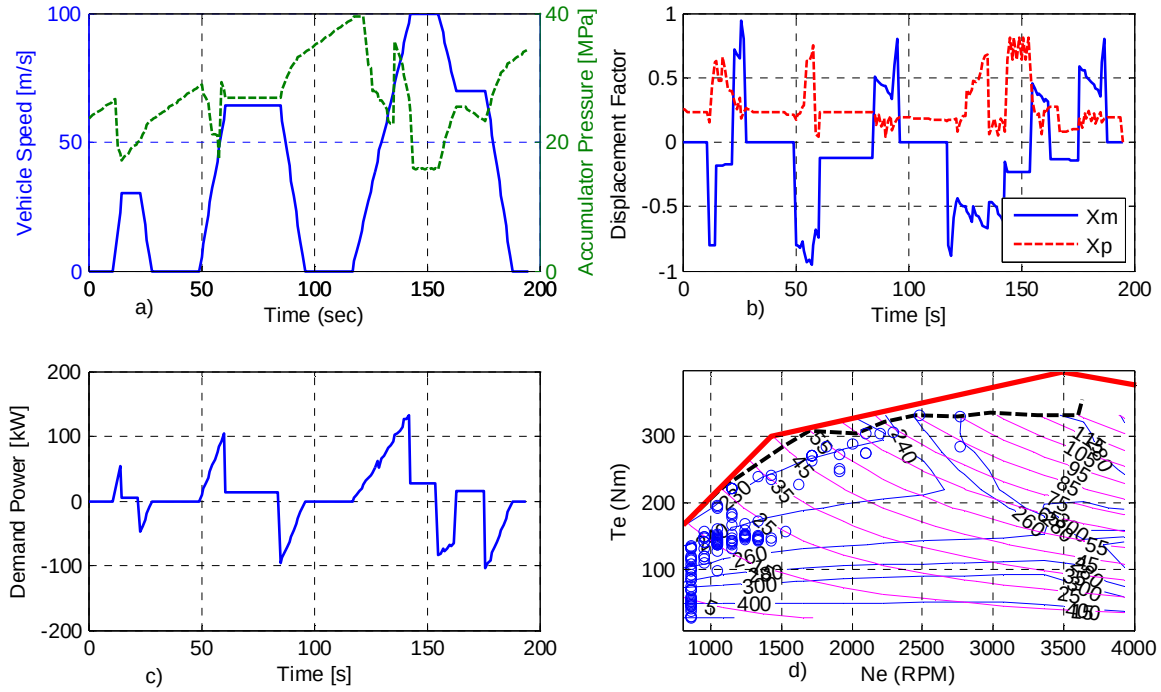

Figure 4-5 DP result plots for modified elementary urban driving cycle a) Vehicle speed and accumulator pressure time history plots, b) Motor and pump displacement factor command history, c) Demand power, d) Engine operating points superimposed on torque-speed map

This shows that DP achieves global minimum as it incorporates future information. It is apparent that for optimum system performance it keeps the accumulator full before a high driving torque requirement comes. Segment J-K is similar to segment F-G. Accumulator discharges most of its energy, as seen from large negative accumulator power during this period, as well as high engine power to maintain a pressure that is necessary for meeting future driving torque requirements. During the high speed cruising, the pressure in the accumulator remains low in preparation for hard braking event ahead and preserving the SOC constrain at the end.

For optimum system performance, the accumulator energy is utilized as much as possible since there is no cost associated with it and it is allowed to vary in a wide range

of values between 16 MPa and 40 MPa. The engine always comes to assist if the pressure available in the accumulator is not enough to drive the vehicle and/or to deliver the required torque at the wheels. The engine operating points stay close to the minimum BSFC lines where the minimum fuel consumption is found for a given power output set by the constraint.

4.1.2 DP Results for FUDS and HWFET Cycles

In this section, the results of implementing the DP algorithm for the FUDS and HWFET cycles will be considered for the cases of with and without engine shutdown and the three accumulator sizes of 10 gal, 15 gal and 20 gal. The fuel economy improvements obtained by implementing the optimal strategy from the DP algorithm in comparison to the conventional powertrain are summarized in Table 4-1.

It can be seen from Table 4-1 that a DP optimized hybrid drive system offers a remarkable fuel economy improvement, in the range of 27-57% on the FUDS and 17-23% on the HWFET, over the conventional drive system. Incorporating engine shutdown in the DP algorithm, i.e. zero engine power output during braking or when the vehicle is at rest, contributes significantly for the fuel economy improvement, particularly in the city (FUDS) cycle. On the HWFET cycle, the fuel economy improvements, with and without engine shutdown, are more or less the same as there is no frequent stop-and-go motion on highway as a result the engine is always on and runs along the minimum BSFC line.

Table 4-1 Fuel economy improvement comparisons of DP algorithm over the conventional drive

	Accumulator volume (gallon)	City cycle (FUDS/UDDS)		Highway cycle(HWFET)	
		Shutdown	W/O Shutdown	Shutdown	W/O Shutdown
Conventional Truck, Ford F150, 4WD, V8, 4.6L, Automatic 4spd [US DOE, fueleconomy.gov] (MPG)	-	-	14	-	18
DP algorithm, Independent Hydrostatic Wheel Drive (4 Motors) (% improvements)	10	56.8	34.4	23.4	21.3
	15	54.2	31.6	21.4	18.54
	20	52.5	27.7	19.5	17.3

In addition, it can be seen from Table 4-1 that the 10 gal accumulator gives a slightly higher fuel economy improvement over both the 15 gal and 20 gal accumulators for both engine idling conditions (with and without shutdown). This could be explained by looking at Figure 4-6. For the case when the pressure in the accumulator is the same and the vehicle is stationary, say for first 20 seconds and between 120^{th} -165^{th} seconds of the cycle, the engine power output of the hybrid system with the 10 gal accumulator is lower than that with the 15 gal accumulator. As the motor power request is zero during this period, the engine power is used to charge the accumulator in anticipation of the acceleration ahead. Since the accumulator power is proportional to its volume as shown

by Eq. (4.8) and a smaller power is required to bring the pressure to the desired level for the system with the 10 gal accumulator than that with 15 gal accumulator. Similarly, the engine power for the system with the 15 gal accumulator is lower than that of the system with the 20 gal accumulator. This low engine power requirement contributes for less fuel use rate and hence better fuel economy. On the other hand, the energy recuperation process of the 10 gal accumulator is better than the one with the 15 and 20 gal accumulators as characterized by their higher SOC during the 120th -165th sec of the cycle. Additional power is delivered to the wheels of the vehicle from the accumulator at the 315th sec of the cycle which ultimately contributes to improving overall efficiency.

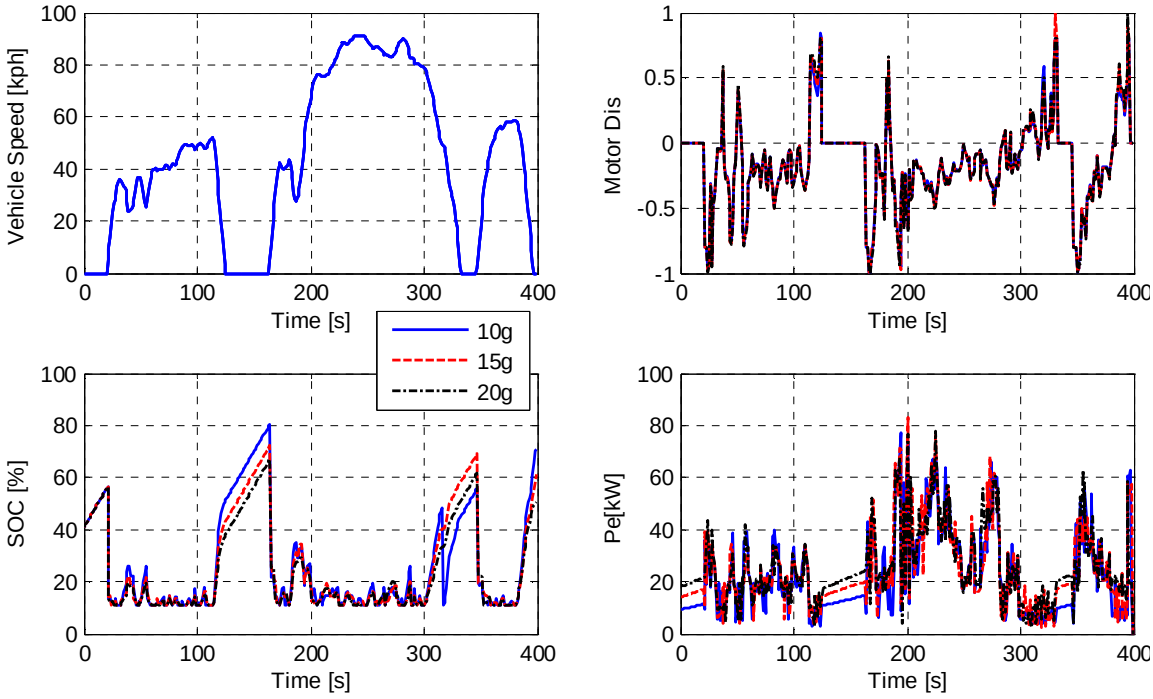

Figure 4-6 DP result comparisons for 10g, 15g and 20g accumulators

The detailed performance results for the 15-gal accumulator are shown in Figure 4-6. Results for the other accumulator sizes are included in the Appendix. It is worth

noting that the optimal engine operating points are superimposed over the minimum BSFC lines of the engine.

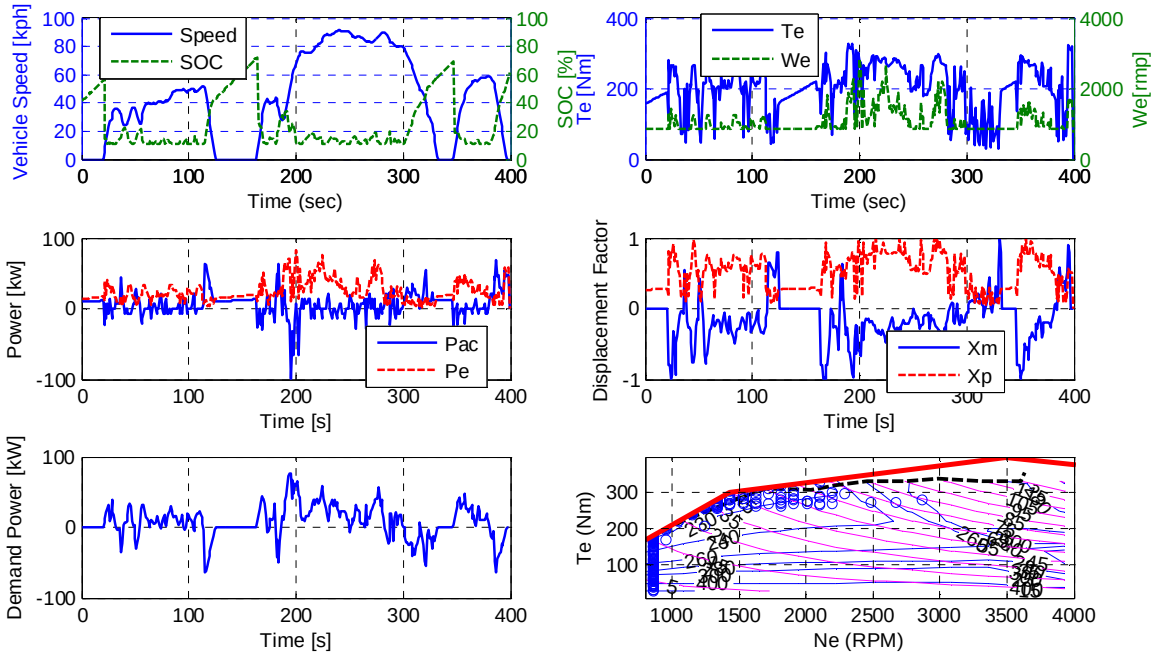

Figure 4-7 DP results of a 15g accumulator for the first 400 seconds of the FUDS cycle without engine shutdown

Figure 4-8 shows system responses and time history plots of the control variables for a known initial state for the 15 gal accumulator which minimizes the fuel consumption over the whole HWFET drive cycle. The SOC of the accumulator starts at 80 % and ends at 80 % to meet the final state constraint imposed in the cost function. The pump works more often close to the maximum displacement limits (higher load) for better efficiency. It can also be observed how the DP algorithm maintains the controls for running the pump at higher load for better efficiency. This is readily noticed from the plot of the displacement factor in Figure 4-8. For the highway cycle, as the requested power/torque demand at the wheels of the vehicle is low and the pressure in the

accumulator remains low, the pump displacement factor stays close to 1 so that the pump always “sees” high load (torque) for maximizing the efficiency.

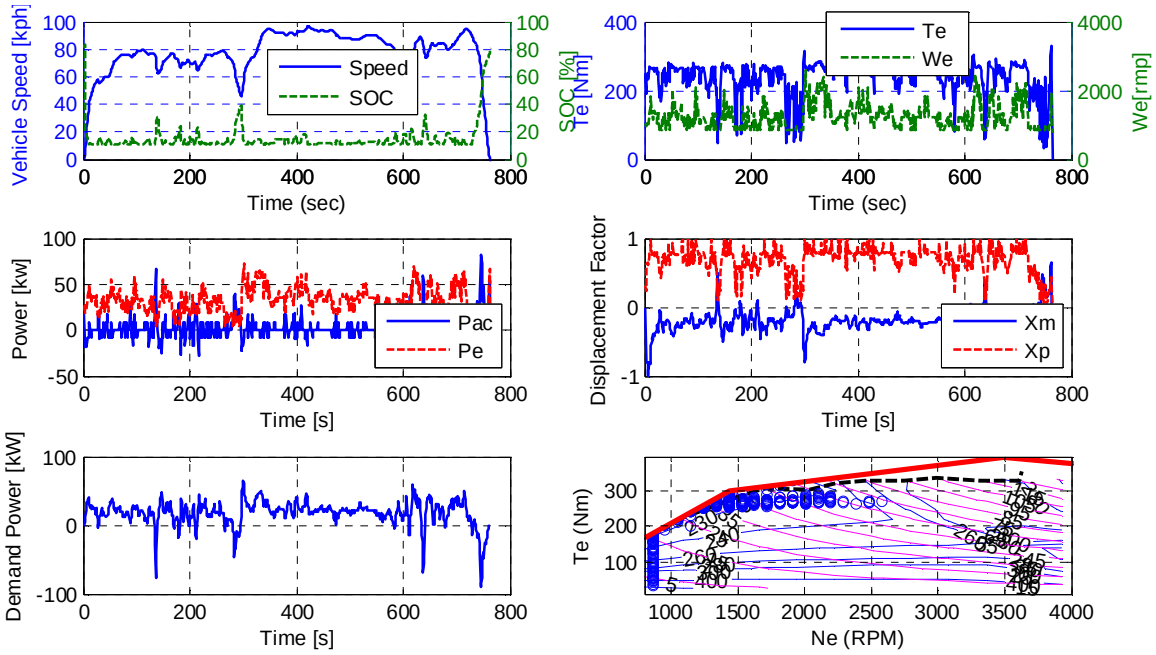

Figure 4-8 DP results of a 15g accumulator for HWFET cycle

4.2 Instantaneous Consumption Minimization Strategy

Ideally, the optimal power distribution between the engine-pump and the accumulator, Eq.3.2, should be determined in such a way that the overall engine fuel consumption over the entire driving cycle is minimized. That is the minimal fuel consumption described by Eq. (4.1) should be found from a global minimization process. For the case where driving cycle is entirely known a prior, dynamic programming is a perfect tool for formulating the control law. However, this is unlikely to happen in the real world applications as the drive cycle (velocity or load profile) is generally not known before the start of the trip. To overcome this drawback, a sub-optimal solution is sought

by replacing the global criterion with a local one using instantaneous equivalent consumption minimization strategy (ECMS).

At all times, this local criterion can be stated as:

$$\min_{u(k)}\left(\frac{d(m_{f\_equ}(t))}{dt}\right) \tag{4.20}$$

where the equivalent fuel use rate cost function $\frac{d(m_{f\_equ}(t))}{dt}$ is defined as the sum of the actual engine fuel consumption rate $\frac{d(m_{f\_ICE}(t))}{dt}$ and the equivalent fuel use rate of storing/discharging power of the hydraulic accumulator $\frac{d(m_{f\_acc}(t))}{dt}$. That is:

$$\frac{d(m_{f\_equ}(t))}{dt} = \frac{d(m_{f\_ICE}(t))}{dt} + \frac{d(m_{f\_acc}(t))}{dt} \tag{4.21}$$

4.2.1 Formulation of ECMS Strategy for the Hydrostatic Drive

In this section of the thesis, a first formulation of the ECMS strategy to hydraulic hybrid (hydrostatic) drive is presented. To understand the working principle of the ECMS strategy, one has to give a close attention to how a series hydraulic hybrid vehicle works (see Figure 4.9).

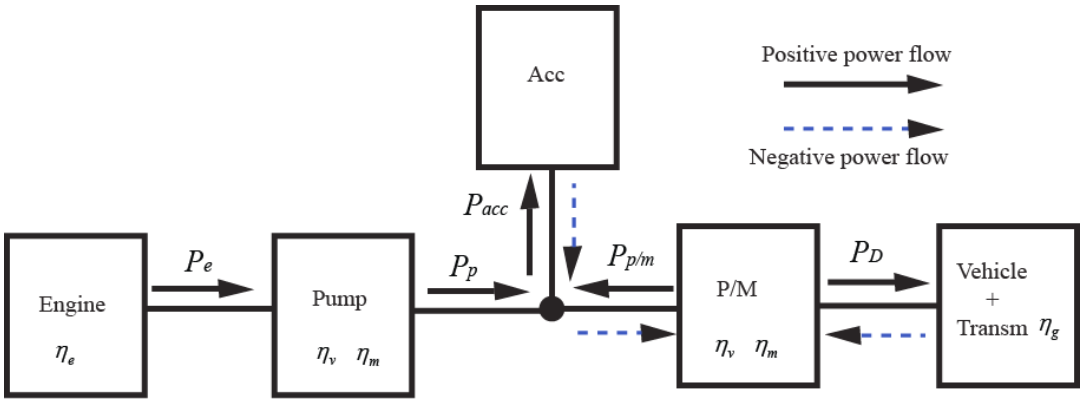

Figure 4-9 schematic representation of simplified hydrostatic powertrain

During vehicle propulsion with the accumulator discharging, the total hydraulic power supplied to the wheel-end P/M is given by the sum of power output from the engine-pump and the hydraulic accumulator. To keep the accumulator pressure within the desired level and provide the required torque at the wheel-end P/Ms, the energy drawn out from the accumulator at present must be recharged in the future. The necessary power to recharge the accumulator needs to be provided then either from regenerative braking and/or the engine-pump set. Conversely, when the accumulator is charging during propulsion, the engine-pump provides the power for the wheel-end P/Ms plus the power is used to charge the accumulator. This extra energy stored in the accumulator at present must later be discharged to maintain the pressure (or SOC) of the accumulator near target level and keep it low and ready for further recuperation that may happen ahead. This in turn means less fuel usage to run the vehicle in the future.

Using this power flow concept, the hydraulic accumulator can be modeled as a virtual auxiliary reversible fuel tank within the hydrostatic powertrain system. This implies that operating the accumulator in discharge mode consumes extra fuel, and

operating the accumulator in charge mode puts back some fuel into the fuel tank for later use. Thus, the basis of the ECMS approach is to associate the hydraulic energy stored in the hydraulic accumulator E_{acc} to an amount of fuel m_{f_acc}. This amount of fuel is estimated by accounting for the average efficiency of the energy path to convert fuel to hydraulic energy as shown by Figure 4-10. As the energy stored in the accumulator is hereby related to an equivalent fuel mass, the power flow in or out of the accumulator P_{acc} is also associated to an equivalent fuel use rate $\frac{d(m_{f\_acc}(t))}{dt}$.

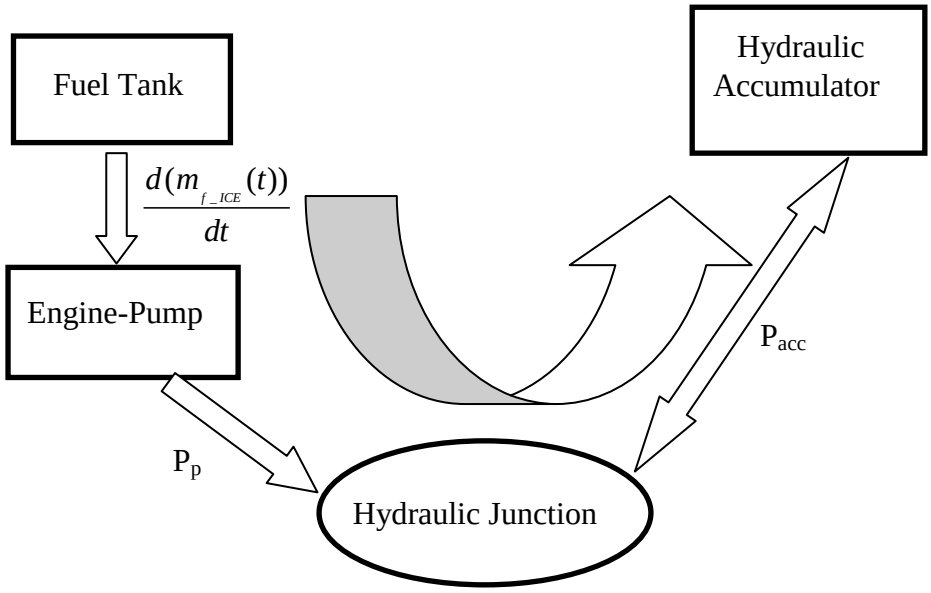

Figure 4-10 Energy flow diagram for the conversion of fuel mass to hydraulic power

The virtual specific consumption of the accumulator, $\overline{SC}_{acc}$(g/kWh), is defined as the average amount of gasoline fuel (g) needed to store 1 kWh of hydraulic energy in the accumulator using the engine-pump as a charger. It can be computed as follows:

$$\overline{SC}_{acc} = \frac{\overline{SC}_{ICE}}{\bar{\eta}_{pump}\bar{\eta}_{char\_acc}} \quad \textbf{(4.22)}$$

where $\overline{SC}_{ICE}$(g/kWh) is the average specific consumption of the engine from fuel to hydraulic energy, $\bar{\eta}_{pump}$ is the average total efficiency of the pump and $\bar{\eta}_{char\_acc}$ is the average charging efficiency of the accumulator.

To calculate the equivalent fuel use for the accumulator, the appropriate charging and discharging efficiency has to be considered. As a result, the equivalent fuel mass flow $\frac{d(m_{f\_acc}(t))}{dt}$ in g/s is calculated as follows:

For positive accumulator power flow (accumulator is charging):

$$\frac{d(m_{f\_acc}(t))}{dt} = -\frac{\overline{SC}_{acc}\, P_{acc}\, \eta_{disch\_acc}}{3600} \quad \textbf{(4.23)}$$

For negative power flow (accumulator discharging):

$$\frac{d(m_{f\_acc}(t))}{dt} = -\frac{\overline{SC}_{acc}\, P_{acc}}{3600\ \eta_{char\_acc}} \quad \textbf{(4.24)}$$

where P_{acc} is the instantaneous power flow in/out of the accumulator (kW), η_{char_acc} is instantaneous charging efficiency and η_{disch_acc} is the instantaneous discharging efficiency of the accumulator. The negative sign is added to comply with the accumulator power flow sign convention adopted above.

Looking at the above equations, the accumulator fuel use rate can take negative, positive or zero values depending on whether the power flow to the accumulator is positive (charging), negative (discharging) or zero. On the other hand, the engine fuel flow rate could take only positive or zero values when the engine is on or off. Therefore, to make the equivalent fuel cost minimum at all time, the engine fuel use should be always close to minimum. This notion confirms the fact that while we minimize the equivalent fuel consumption, the instantaneous engine fuel use is also minimized implicitly at all time.

In general, the equivalent fuel consumption minimization strategy is based on the assumption of quasi-static behavior of the system [45]. This assumption ignores fast dynamics of the system. In the present work, this implies the engine dynamics are neglected and that the torque and speed of the engine exactly matches the torque and the speed of the pump. Since $T_e = T_p$ and $\omega_e = \omega_p$, then $\eta_{eng}(T_e, \omega_e)$ can also be expressed as $\eta_{eng}(x_p, \Delta p_p, \omega_p)$.

The minimum mass flow rate of the engine is a function of engine power output whereas the accumulator equivalent fuel use rate is a function of accumulator power output/input. Rewriting the equivalent fuel consumption equation, we have:

$$\frac{d(m_{f\_equ}(t))}{dt} = \frac{d(m_{f\_ICE}(P_e(t)))}{dt} + \frac{d(m_{f\_acc}(P_{acc}(t)))}{dt} \qquad \textbf{(4.25)}$$

Given that the accumulator power is given by $P_{acc}(t) = P_p(t) + P_{p/m}(t)$, plugging it in the above equation and dropping the independent variable “t” as it is implicitly known:

$$\frac{d(m_{f\_equ})}{dt} = \frac{d(m_{f\_ICE}(P_e))}{dt} + \frac{d(m_{f\_acc}(P_p + P_{p/m}))}{dt} \quad \textbf{(4.26)}$$

It is known that the Brake Specific Fuel Consumption (BSFC) of the engine is related to the engine efficiency through a constant: $BSFC = \frac{C}{\eta_{eng}}$, where C is a constant, which for gasoline engine takes the value of C = 84.7 (g/kWh). Then, the engine fuel flow rate $\frac{d(m_{f\_ICE})}{dt} = (BSFC)P_e$, but $P_e = \frac{P_p}{\eta_p}$, where $\eta_p(x_p, \Delta p_p, \omega_p)$ is total efficiency of the pump.

$$\frac{d(m_{f\_ICE})}{dt} = \frac{84.7}{\eta_{eng}} \frac{P_p}{\eta_p} \quad \textbf{(4.27)}$$

For the engine fuel mass flow rate to be minimum the product ($\eta_e \eta_p$) should be maximum at the corresponding pump power output. This maximum overall efficiency of the engine-pump set (or minimum $\frac{d(m_{f\_ICE})}{dt}$) and the corresponding x_p and ω_p are calculated off-line and are stored as a function of Δp across the pump and pump power output (P_p).

To enforce component limitations and ensure safety, the physical constraints that have been taken into consideration during DP optimization, Eq. (4.19), are considered here. Finally, the equivalent consumption strategy can be written as:

$$\frac{d(m_{f\_equ})}{dt} = \frac{d(m_{f\_ICE}(P_p, \Delta p))}{dt} + \frac{d(m_{f\_acc}(P_p + P_{p/m}))}{dt} \quad \textbf{(4.28)}$$

From a given driving cycle, at each instant of time, the drivers' motor power request is as assumed known. At the same time, the SOC of the accumulator is estimated through the gas pressure. By searching through all possible values of the pump power output, the instantaneous power flow distribution with lowest equivalent fuel cost can therefore be selected using the formulation in Eq. (4.28).

For a hydrostatic/hydraulic hybrid drive system, the SOC of the accumulator is allowed to vary in a wide range between the minimum, say 10 %, to the maximum, say 100% to exploit two attractive features of the gas-charged accumulator: 1) that it can handle high charge and discharge rates 2) it does not have depth of charge/discharge related problems as do electrochemical batteries. As a result, keeping the SOC of the accumulator within a narrow window is not useful from the point of view of maximizing the fuel economy of hydraulic hybrid vehicle. On the other hand, due to its low energy density of hydraulic accumulator, charging it from the engine-pump side is not recommended, unless and otherwise the pressure in the accumulator is too low to maintain the desired torque at the P/M end. Due to these reasons, the penalty functions term used to bias the equivalent fuel use of electrochemical batteries up or down as a function of SOC as proposed by [27, 46] for electric hybrid vehicles isn't directly applicable for the hydrostatic system considered in this work. The penalty function has to be modified to account for the wide range variation of accumulator SOC or a new approach/method must be formulated.

In this thesis, as a first application to hydraulic hybrid drives, a simple thermostatic on-off strategy is implemented to see and establish baseline results for the

ECMS strategy (Figure 4-11). When the engine-pump is turned-off, the pump power output is zero and when the engine-pump is turned-on the pump power output is chosen to minimize the instantaneous equivalent fuel consumption.

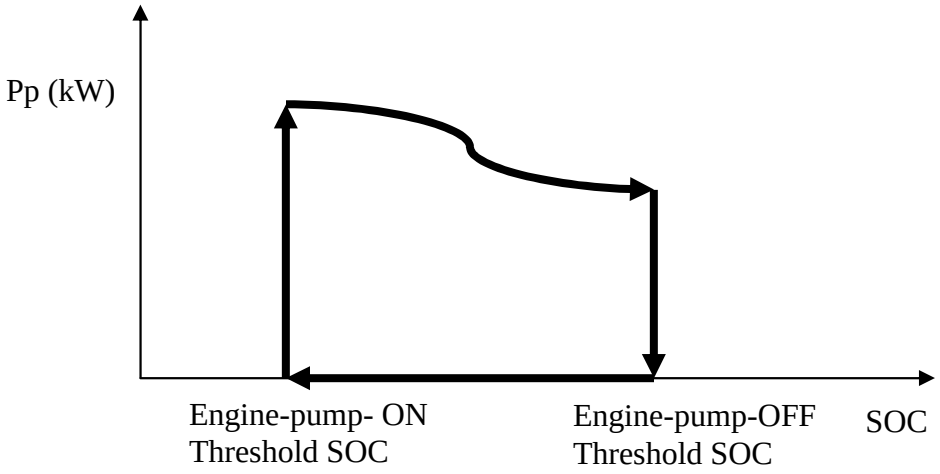

Figure 4-11 ECMS power management strategy pictorial representation

4.2.2 Fuel Economy Results and discussion of ECMS Strategy

The ECMS strategy formulated above is implemented to drive a series hydraulic hybrid vehicle in a forward-facing Simulink environment to investigate the fuel economy improvement potential. The ON-OFF threshold parameters of the ECMS strategy are chosen to comply with the Engine-ON and Engine-OFF threshold SOC points selected for the rule-based strategy in Chapter 3. Table 4-2 summarizes and manifests the expected fuel economy improvement of the ECMS strategy over the conventional drive for city and highway cycles, for different accumulator sizes and number of wheel-end P/Ms

Table 4-2 ECMS fuel economy improvement over the conventional drive.

	Accumulator volume (gallon)	City cycle (FUDS/UDDS)	High way cycle(HWFET)
Conventional Truck, Ford F150, 4WD, V8, 4.6L, Automatic 4spd [US DOE, fueleconomy.gov] (MPG)	-	14	18
Independent Hydrostatic Wheel Drive (4 Motors, ECMS) (% improvements)	10	41.1	12.8
	15	41.1	11.2
	20	41	10.1
Independent Hydrostatic Wheel Drive (2Motors, ECMS) (% improvement)	10	59.6	27.6
	15	59.7	26.2
	20	60.6	24.7

The percentage fuel economy improvement of the proposed strategy shows an extensive potential over the conventional drive, especially for the city drive cycle. Unlike the results from the rule-based strategy, accumulator size doesn't have a significant effect on fuel efficiency for city cycle. This has more to do with the nature of the optimization. Regardless of the accumulator size, the ECMS strategy finds the best engine-pump power for that point. On the other hand, the fuel economy improvement of highway cycle with different accumulator size reveals the fact that for the case where there is no frequent stop-and-go-motion, reducing the rolling resistance (the GVW of the system) has an ultimate contribution on the fuel economy improvement.

For both city and highway driving schedules, reducing the number of wheel-end P/Ms for propulsion has a great impact on the fuel economy improvement as the

efficiency of the P/M unit increases and is hence the overall efficiency. This is the same as was demonstrated with the rule-based strategy.

CHAPTER FIVE

5 COMPARATIVE SUMMARY AND DISCUSSION OF HYBRID MANAGEMENT STRATEGIES

In this chapter, the three power management strategies detailed in Chapter 3 and Chapter 4 are compared using simulations of the system models outlined in Chapter 2. The comparative results are presented considering different accumulator sizes with engine shutdown during idling for the city (FUDS) and highway (HWFET) driving cycles.

The fuel economy results are summarized in Table 5-1. Figure 5-1 and Figure 5-2 show these results graphically. It can be seen from Figure 5-1 that, for the FUDS cycle, the DP optimized hybrid vehicle gives a fuel economy improvement of 20% over that of the percentage improvement obtained by using rule-based power management strategy where as the ECMS strategy gives a fuel economy improvement of more than 7% over the rule-based one. And from Figure 5-2, for the HWFET cycle, the DP optimized hybrid drive gives a fuel economy improvement of 15% more than what is obtained by rule-based power management strategy while ECMS gives more than 5% over the rule-based strategy.

.

Table 5-1 comparison of power management strategies on the performance of fuel economy improvement over the conventional drive

	Accumulator size (gallons)	City cycle (FUDS/UDDS)	Highway cycle(HWFET)
Conventional Truck, Ford F150, 4WD, V8, 4.6L, Automatic 4spd (% improvements)	-	0	0
Rule-Based (4 Motors) (% improvements)	10	32	7.3
	15	34	6.3
	20	32	5
DP algorithm (4 Motors) (% improvements)	10	56.8	23.4
	15	54.2	21.4
	20	52.5	19.5
ECMS strategy (4 Motors) (% improvements	10	41.1	12.8
	15	41.1	11.2
	20	41	10.1

Had the 2WD system been implemented using DP algorithm to drive the vehicle; the fuel economy would have been increased further. For instance, considering engine shutdown with a 2-motor independent hydrostatic drive and a 20 gal accumulator (shown in Appendix C), it is possible to achieve as much as a 74% fuel economy improvement over the conventional drive. This is because, as already pointed out in chapter 3 section 3.2.1.3.1, in 2-motor drive, each wheel-end P/M takes up larger individual loads than in 4-motor drive. This increases their operating efficiency and subsequently contributing to the overall system efficiency.

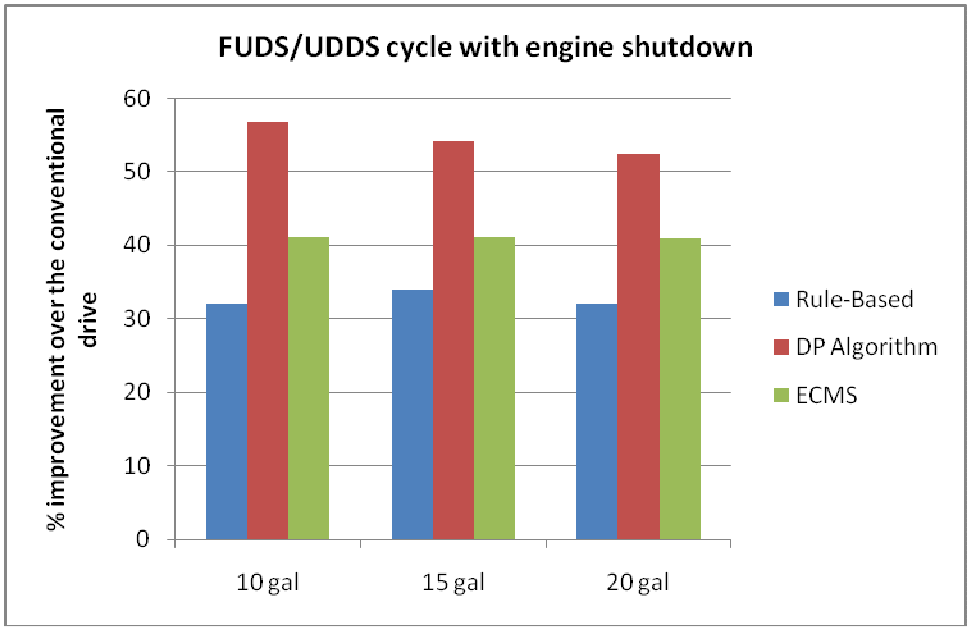

Figure 5-1 Comparison of power management strategy on fuel economy improvement for city cycle

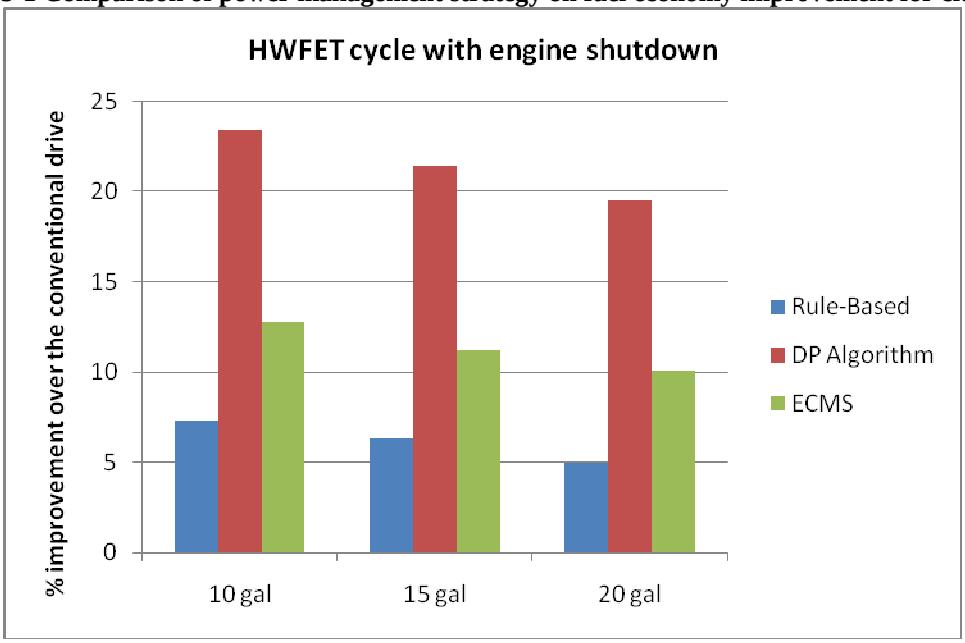

Figure 5-2 Comparison of power management strategy on fuel economy improvement for highway cycle

The reason for achieving best or globally optimal results with DP algorithm is its ability to "see and predict" or "preview" the future events ahead by explicitly considering

the future speed trajectory as known and searching through all alternative operating points for the power system and its components. It then prepares all the components to act accordingly for optimum power split while keeping their operating points close to their respective maximum efficiency region at all times.

On the other hand, by formulating and implementing the instantaneous consumption minimization principle, a sub-optimal solution has been generated with a potential of being implemented in the real time application.

A further investigation of the operating points can be done using the results in Figure 5-3. It shows a comparison of the three power management strategies considering the fractions of total operating time spent within certain ranges for the pump displacement. The HWFET cycle is considered for the system with 15 gal accumulator. The figure shows that the pump was running with a displacement above X_p=0.7 only 65% of the time for DP strategy compared to only 12% of the time for the rule-based strategy. Again, recall that higher displacement is always favorable for better efficiency of the pump/motor unit. This exemplifies how DP optimizes the operating efficiency of each component to increase the overall efficiency of the system. Furthermore, due to the inherent “preview” in the DP algorithm, recuperation is more efficient as the accumulator pressure is set to low for maximum utilization in anticipation of braking events ahead.

For ECMS strategy, the engine-pump was more often running (almost half of the total time) with a displacement factor of around 0.6 or else it was set to zero for the rest of the total time of operation. This pump displacement was chose for the sake of maximizing the engine-pump unit efficiency as whole at each instant of time when the

engine-pump is turned on. Otherwise keeping it to zero as much as possible definitely reduces the fuel use as no fuel consumption is associated during engine-off.

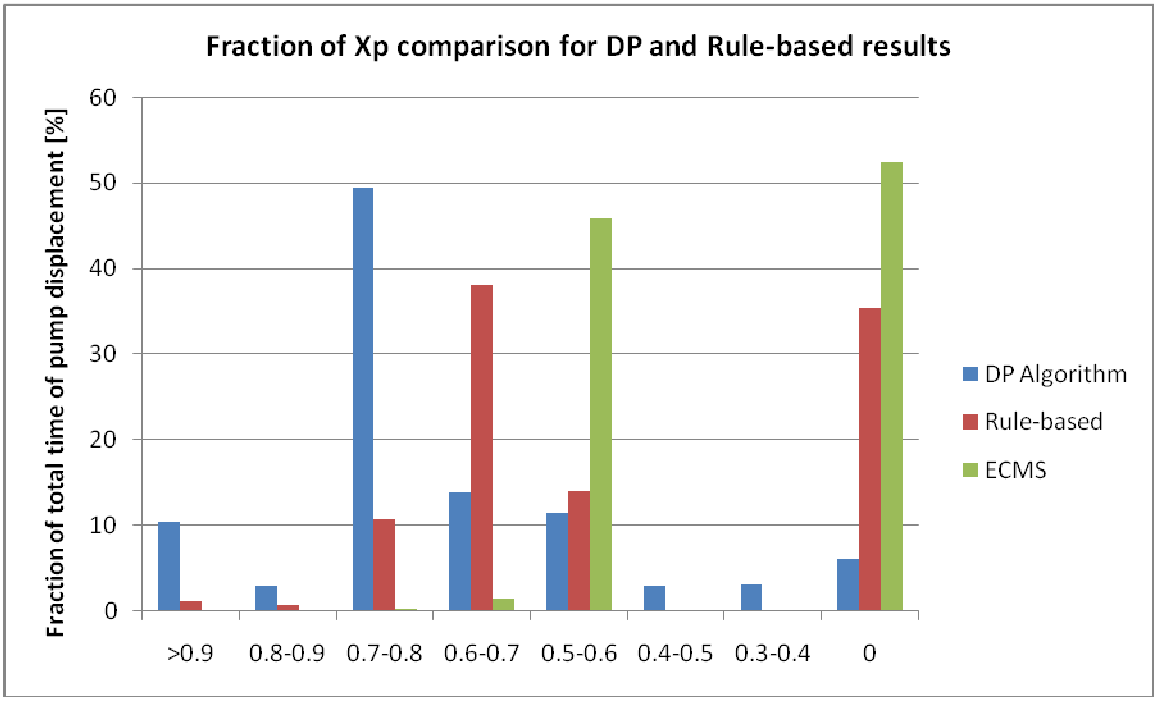

Figure 5-3 Comparison of cumulative effect on fraction of total operating time spent within the pump displacement intervals for the two types of power management strategies for 15 gal accumulator size

In contrast to the DP algorithm, the rule-based power management strategy doesn't "preview" the future ahead of time and hence it couldn't prepare the power sources for optimum power split as well as effective regeneration. Furthermore, the rule-based power management strategy doesn't consider the efficient use of all of the individual power sources (engine pump and accumulator) and power converters (pumps/motors). It only considered optimizing the engine operation. This is obviously not adequate to optimize the overall system performance. However, a major attribute of

the rule-based strategy is it has a causal orientation and can easily be implemented in real-time as a feedback control law monitoring the state-of charge online.

Despite the potential benefits presented and discussed above, the DP algorithm is not causal and cannot be implemented in real-time control. For the DP algorithm to generate the optimal control variables the driving schedule over which the optimization is performed must be entirely known at the beginning of the trip, which is unlikely for real time application. Moreover, the huge computational time requirement makes DP not feasible for practical implementation. As an example for our simulation, DP algorithm takes 17 hours to generate the time varying state feedback law for one complete highway cycle with Genuine Intel(R) CPU T2500 @ 2.0 GHz processor speed machine.

CHAPTER SIX

6 CONCLUSION AND FUTURE WORK

In this thesis, a detailed, causal or forward-facing model of a proposed hydrostatic (series hydraulic hybrid) independent wheel drive system has been outlined. It included models of the hydrostatic drive system components (i.e. pump, pump/motors, accumulators, hydraulic junctions and transmission lines, and the IC engine) and their causal interconnection. The drive system was then integrated with a longitudinal vehicle dynamics model suitable for evaluating the fuel/energy use and acceleration performance of the drive system.

The overall system model was primarily used to evaluate three hybrid power management strategies: a rule-based strategy, a globally optimal (drive cycle optimal) using dynamic programming algorithm, and instantaneous optimization (ECMS) strategy. The rule-based strategy uses the accumulator SOC as a sole variable to determine the power split between the engine-pump and the accumulator in such a way that the engine is constrained to operate along its minimum BSFC line when it is turned-on. Dynamic programming uses the principle of optimality, proposed by Bellman, to determine the time-varying state feedback law with the objective of minimizing the total fuel use of the engine along the entire trip and generate the globally minimum solution. The instantaneous equivalent consumption minimization strategy (ECMS), on the other hand, translates the accumulator power use into an equivalent fuel use rate at each instant of

time and then determines the power split that gives the minimum equivalent fuel use rate for the whole system.

6.1 Summary of Results Using Rule-Based Strategy

In most of simulations of the test vehicle in this thesis, the vehicle analyzed was considered to be about 20% heavier than the baseline vehicle in order to take into account the upgraded capability of the hybridization and allow for the weight of the added hydrostatic system components.

Simulation results showed that a well-tuned rule-based strategy leads to a fuel economy improvement for the 4 hydrostatic system over the conventional drive system of more than 30% and 5% on the city (FUDS) and highway (HWFET) drive cycles, respectively. The improvement is higher on the city cycle than the highway cycle, because unlike the highway cycle, the city cycle is characterized by frequent stop-and-go motion offering many opportunities for recuperating some fraction of the kinetic energy of the vehicle during braking and subsequent use of this energy for propulsion. This energy recuperation and re-use reduces fuel use in the engine. Moreover, the frequent stop-and-go-motion in the city cycle allows shutdown of the engine when it is not need, especially during extended idling period. These conditions contribute for the significant fuel economy improvement in the city cycle.

The effect of number of motors on the performance of fuel economy improvement was also investigated using the rule-based power managment strategy. Simulation results show that the 2-motor drive system offers a 50% fuel economy improvement over the

conventional drive in the city cycle. This is a 20% increment over what was found for a 4-motor drive system on the same drive cycle. The higher fuel economy improvement with the 2-motor drive is attributed to the fact that when the vehicle is propelled by just the 2-motors, the individual motors take up higher load (torque) for most of the time. This higher load (torque) is favorable for increasing the efficiency of hydraulic machines. However, the acceleration performance suffers when using 2-motors, as the peak performance the system was sized for assumed the 4-motor operation. Furthermore, 2-motor propulsion gives fewer actuation choices for implementing vehicle stability control with independent drive.

Another issue that was investigated using the rule-based strategy was the effect of accumulator size on the performance of the vehicle. It was found that, for the city cycle, the 15 gal accumulator gave better fuel economy results than the 10 gal and 20 gal accumulators. This is because the 15 gal accumulator size balances the tradeoff between the frequent loss of energy recovery-opportunities due to frequent friction brake activation, as happens with the smaller 10g accumulator, and the energy loss in rolling resistance (and some inertia) due to increased GVW, as happens with 20 gal accumulator.

6.2 Summary of Results Using Optimization-Based Strategies

To overcome some of the drawbacks of the heuristically tuned rule-based strategy and to see how "close" it comes to the global optimum solution, a dynamic programming (DP) algorithm was first formulated and implemented for the hydrostatic powertrain. Due to its inherent use of "preview", the results obtained by DP are optimal for the whole trip

or drive cycle and can therefore serve as benchmarks to which results from other strategies can be compared and evaluated. In addition to being non-causal, even when the drive cycle could be known apriori, the computational intensity of the DP algorithm limits its use in real-time hybrid power management.

The DP optimal strategy applied to the hydraulic hybrid drive leads to a fuel economy improvement over the conventional drive of 50% and 20% on the city (FUDS) and highway (HWFET) cycles, respectively. A closer look at the comparative percentage fuel economy improvements of the DP optimal strategy over the rule-based strategy (20% on FUDS, and 15% on HWFET) indicated that the selected control threshold parameters for the rule-based power management strategy were tuned more favorable for the city cycle than the highway cycle. However, it is evident that a gap exists in the achievable fuel economy improvement with the rule-based strategy compared to the DP globally optimal solution.

This gap motivated the consideration of the third approach: instantaneous optimization or ECMS. In this, the goal is to take into account component efficiencies and constraints much like the global optimization problem, while attempting to instantaneously optimize the total energy use when deciding the power split between the accumulator and the IC engine-pump set. One of the attractive features of this instantaneous optimization method is that it can be implemented in real-time applications. In this work, the ECMS computation has been incorporated in the causal or forward-facing Simulink model of the complete dynamics of the hydraulic hybrid drive system.

Simulation results showed that the proposed ECMS strategy applied to the 4 motor hydrostatic drive gave fuel economy improvements over the conventional drive of nearly 40% and 10%, on the city (FUDS) and highway (HWFET) cycles, respectively. This is a promising result given the simplifying assumptions on the average efficiencies adopted for coming up with equivalence factors for this first implementation of ECMS to hydraulic hybrids.

6.3 Future Work

To the best of the author's knowledge, the implementation of ECMS to hydraulic hybrids has not been reported in previous work. The author has laid out the foundation for conducting further studies on this. Future work will refine the strategy specifically recognizing the low energy density of the storage system in hydraulic hybrids. Furthermore, the average specific consumption and the average efficiencies values of the engine-pump set and the hydraulic accumulator should are not remain constant for all drive cycles, as was assumed in this work. These values vary at each instant of time with the driving cycle. The impact of the threshold SOC engine-pump-on-off points of the ECMS strategy on the fuel economy improvement should be investigated and, possibly, a more continuous SOC-dependent weighing factor should be derived specifically for hydraulic hybrids.

APPENDICES

APPENDIX A

Nomenclature

A = vehicle frontal area

A_p = pipe cross sectional area

Aw = effective accumulator wall area

C_D = drag coefficient

c_f = constant pressure specific heat of foam

c_v = constant volume specific heat of gas

D = maximum displacement of pump/motor

F_x = longitudinal tire force

g= gravitational constant

h = heat transfer coefficient

J_{weq} = inertia of motor/wheel referred to wheel

J_{eq} = equivalent inertia of the pump/engine

m = total vehicle mass

m_f = mass of foam in accumulator

m_g = mass of the gas in accumulator

P_e = engine power

p_g = gas pressure

p_j = junction pressure

p_p, p_m = pump/motor pressure

Q_{acc} = accumulator flow rate

Q_{ap}, Q_{am} = actual pump/motor flow rate

Q_i = ideal flow rate

R_w = effective wheel radius

T_{ap}, T_{am} = actual pump/motor torque

T_i = ideal torque

T_L = load (pump) torque

T_w = accumulator wall temperature

V = vehicle speed

v = specific volume of the gas

V=accumulator volume

V = vehicle speed

x = displacement factor for pump/motor

ω_{e_des} , $\omega_{e/p}$ = desired/ actual rotational speed of the engine-pump

ω = rotational speed of wheel i

ρ = density of air

τ = thermal time constant

η_v = volumetric efficiency

η_m = mechanical efficiency

Δp= pressure difference across pump/motor

m_{f_equ}= equivalent fuel use

m_{f_ICE}= ICE mass fuel use

m_{f_acc}= accumulator equivalent mass fuel use

$\overline{SC}_{ICE}$ = ICE specific fuel consumption

$\overline{SC}_{acc}$ = accumulator specific fuel consumption

$\bar{\eta}_{char\_acc}$ = average accumulator charging efficiency

$\bar{\eta}_{dis\_acc}$ = average accumulator discharging efficiency

BSFC= ICE brake specific fuel consumption

.

APPENDIX B

Main Parameters Specifications

Table B-1 Vehicle parameters

Vehicle mass GVWR[lbs](Kg) - Class 2 truck	8000 (3629)
Drag coefficient, Cd	0.414
Frontal area, Af [m^2]	2.4
Rolling resistance coefficient , f0	0.015
Wheel inertia , Jw [Kg-m^2]	1.1
Motor inertia, Jm [Kg-m^2]	0.0042
Transmission ratio b/n the motor and the wheel, ig	4.0
Tire type	LT265/75R16
Wheel radius, Rw [m]	0.402

Table B-2 Engine specifications

Engine type	4.6L Triton V8
Bore X stroke (in)	3.55 X3.54
Displacement (L)	4.600
Rated power (kW)@ 4750 rpm	172(231 hp)
Compression ration	9.3:1
Torque (lb-f)@ rpm	293 @3500
Fuel system	Sequential multi-port electronic fuel injection (SEFI)

Table B-3 Accumulator parameters

Accumulator size[g]	10, 15, 20
Pre-charge pressure [Mpa]	13
Low pressure corresponding zero SOC [MPa]	13.2
Pre-charge temperature(k)	320
Maximum pressure [MPa]	40

Table B-4 Axial piston swash plate pump parameters

Pump displacement [cc/rev]	125
Maximum speed of the pump[rpm]	2850
Nominal pressure [bar]	400
Peak pressure [bar]	450
Intermittent max speed [rpm]	3450
Pump inertia [Kg-m^2]	0.0232

Table B-5 Bent axis P/M parameters

Pump/Motor displacement [cc/rev]	55
Maximum speed of the pump/motor[rpm]	4450
Nominal pressure [bar]	400
Peak pressure [bar]	450
Motor inertia [Kg-m^2]	0.0042

.

APPENDIX C

Additional System Simulation Results

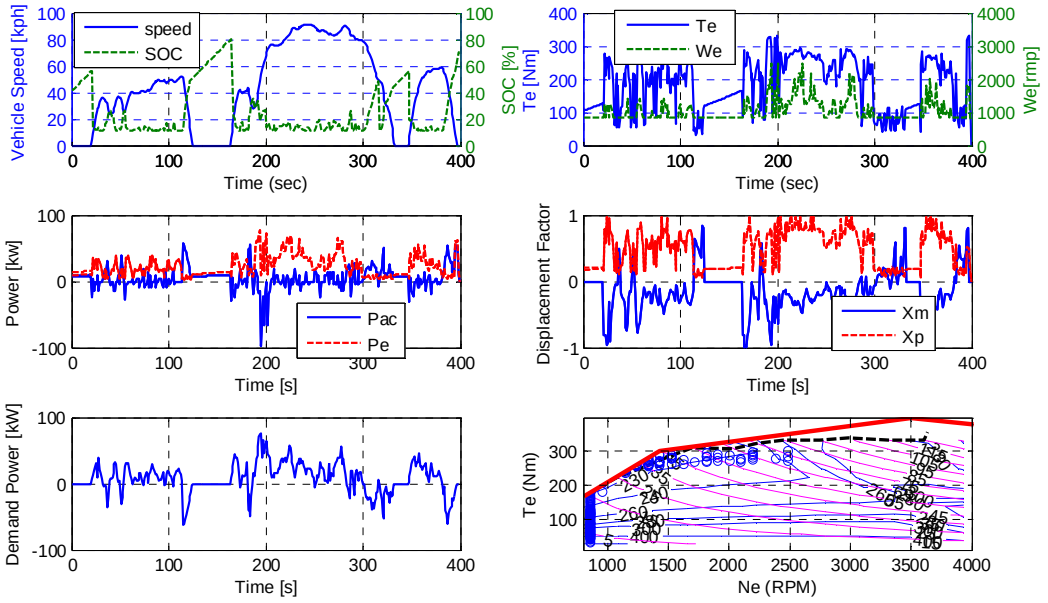

Figure C-1 DP results of a 10g accumulator for the first 400 seconds of the FUDS cycle without engine shutdown

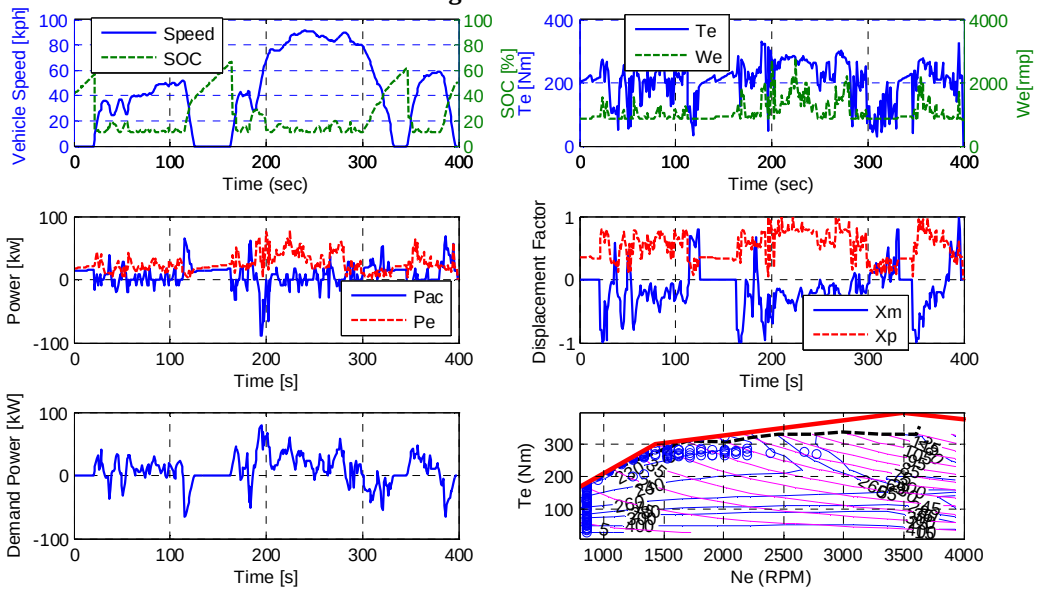

Figure C-2 DP results of a 20g accumulator for the first 400 seconds of the FUDS cycle without engine shutdown

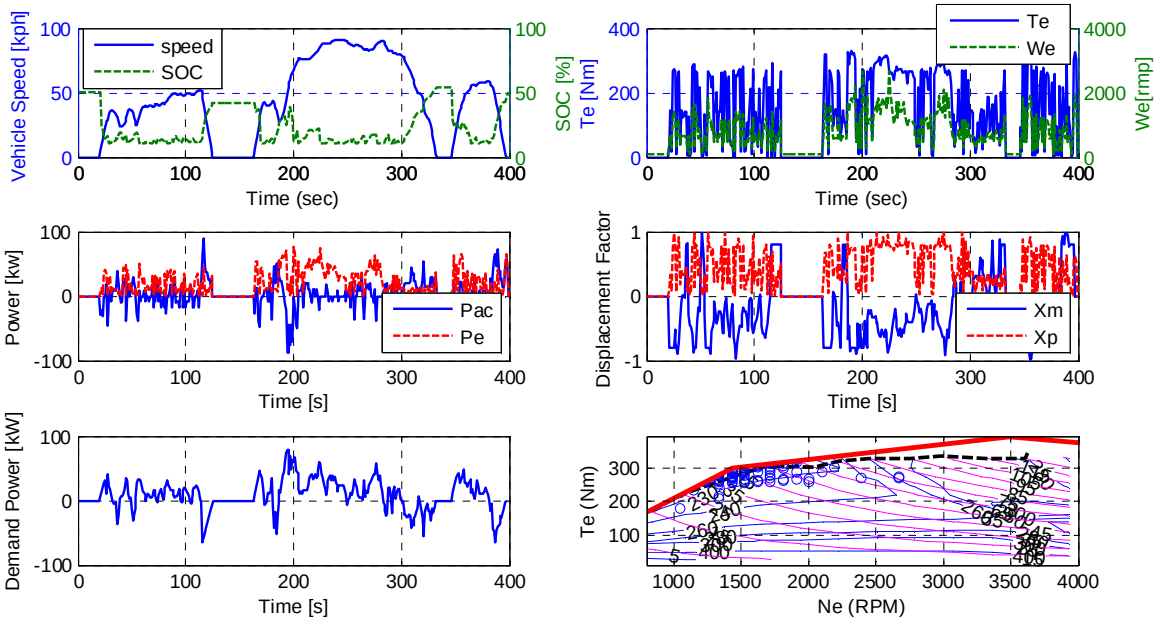

Figure C-3 DP results for a 2-motor drive and 20g accumulator with engine shutdown

REFERENCES

1. Baumann, B.M., et al., *Mechatronic Design and Control of Hybrid Electric Vehicles.* IEEE/ASME Transactions on Mechatronics 2000. **Vol. 5,NO. 1**.
2. Baseley, S., et al., *Hydraulic Hybrid System for Commercial Vehicles* in *Commercial Vehicle Engineering Congress and Exhibition*. 2007: Rosemont, Illinois.
3. NextEnergy. *http//www.nextenergy.org/industrial service/hybrid hydraulics.asp*. 2008 [cited 2008 07/02].
4. Pourmovahed, A., *Vehicle Propulsion Systems with a Hydraulic Energy Storage: A Literature Survey.* International Journal of Vehicle Design, 1991. **Vol. 12**(4): p. 378-403.
5. Hewko, L.O. and T.R. Weber, *Hydraulic Energy Storage Based Hybrid Propulsion System for a Terrestrial Vehilce.* 1990. **Vol. 4**: p. 99-105.
6. Nakazawa, N., et al., *Development of a Braking Energy Regeneration System for City Buses*, in *SAE paper number 872265*. 1987.
7. Molla, S., J. Sill, and B. Ayalew, *Hydrostatic Wheel Drives for Vehicle Stability Control*, in *SAE International World Congress*. 2010: Detroit, Michigan.
8. Karogal, I. and B. Ayalew, *Independent Torque Distribution Strategies for Vehicle Stability Control*, in *SAE World Congress*. 2009: Detroit, MI.
9. Goodarzi, A. and E. Esmailzadeh, *Design of a VDC System for All-Wheel Independent Drive Vehicles.* IEEE/ASME Transactions on Mechatronics, 2007. **Vol. 12**(6): p. 632-639.
10. Jeongmin Kim, H.K., *Electric Vehicle Yaw Rate Control using Independent In-Wheel Motor*. IEEE Trans. Control System Technology, 2007.
11. L.Matheson, P. and J. S.Stecki. *Development of Hybrid Diesel-Hydraulic System for Large Comercial Vehicles* in *The Eighth Scandinavian International Conference on fluid power, SICFP'03*. 2003. Tamper, Finland.
12. Matheson, P. and J. Stecki. *Development of Hybrid Diesel-Hydraulic System for Large Comercial Vehicles* in *The Eighth Scandinavian International Conference on fluid power, SICFP'03*. 2003. Tamper, Finland.
13. Ven, J.D.V.d., M.W. Olson, and P.Y. Li. *Development of a Hydro-Mechanical Hydraulic Hybrid DriveTrain with Independent Wheel Torque Control for an Urban Passenger Vehicle*. in *Proceedings of the International Fluid Power Exposition*.
14. Kumar, R. and M. Ivantysynova. *An Optimal Power Management Strategy for Hydraulic Hybrid Output Coupled Power-Split Transmission*. in *Proceedings of the ASME 2009 Dynamic Systems and Control Conference*. 2009. Hollywood, California, USA.
15. Z.Filipi and Y.J.Kim, *Hydraulic Hybrid Propulsion for Heavy Vehicles:Combining the Simulation and Engine-in-the-Loop Techniques to*

maximize the Fuel Economy and Emission benifit in *IFP international conference*. 2009: Oil & Gas Scince and Technology-Rev. IFP.

16. Filipi, Z., et al., *Combined optimization of design and power management of the hydraulic hybrid propulsion system for the 6X6 medium truck.* Int. J. of Heavy Vehicle Systems, 2004. **Vol. 11**(3/4): p. 372-402.
17. Brahma, A., Y. Guezennrc, and G. Rizzoni, *Optimal Energy Mangement in Series Hybrid Electric Vehicles,* in *Proceedings of the American Control Conference* 2000: Chicago, IL. p. 60-64.
18. Wu, B., et al., *Optimal Power Management for a Hydraulic Hybrid Delivery Truck.* Vehicle System Dynamics, 2004. **Vol. 42**(1/2): p. 23-40.
19. Jalil, N., N. A.Kheir, and M. Salman, *A Ruled-Based Energy Management Strategy for a Series Hybrid Vehicle* in *Proceeding of the American Control Conference* 1997: Albuquerque, NM. p. 689-693.
20. Lin, C.-C., et al., *Power Management Strategy for a Parallel Hybrid Electric Truck.* IEEE Transactions on Control Systems Technology, 2003. **Vol. 11**(NO. 6): p. 839-849.
21. Musardo, C., G. Rizzoni, and B. Staccia, *A-ECMS: An Adaptive Algorithm for Hybrid Electric Vehicle Energy Management*, in *Proceeding of the 44th IEEE Conference on Decision and Control and the European Control Conference*. 2005. p. 1816-1823.
22. Kim, Y.J. and Z. Filipi. *Simulation Study of a Series Hydraulic Hybrid Propulsion System for a LIght Truck*. 2007. SAE Paper No. 2007-01-4151.
23. Baumann, B.M., et al., *Mechatronic Design and Control of Hybrid Electric Vehicles.* IEEE/ASME TRANSACTIONS ON MECHATRONICS, 2000. **VOL. 5,NO. 1**.
24. Farrall, S.D. and R.P. Jones. *Energy management in an automotive electric/heat engine hybrid powertrain using fuzzy decision making.* in *Proceedings of the 1983 iInternational Symposium on Intelligent Control*. 1983. Chicago, Illinois.
25. Rotenberg, D., A. Vahidi, and I. Kolmanovsky, *Ultracapacitor Assisted Powertrains: Modeling, Control, Sizing, and The Impact on Fuel Economy*, in *American Control Conference*. 2008: Westin Seattle Hotel, Seattle, Washington, USA.
26. G.Paganeli, et al., *Equivalent Consumption Minimization Strategy for Parallel Hybrid Powertrain.* IEEE Xplore, 2002: p. 2076-2081.
27. Liu, J. and H. Peng. *Control Optimization for a Power-Split Hybrid Vehicle*. in *Proceedings of the 2006 American Control Conference*. 2006. Minneapolis, Minnesota, USA.
28. G.Paganelli, et al., *Simulation and assessment of power control strategies for a parallel hybrid car* Proceedings of the Institution of Mechanical Engineers, Part D: Journal of Automobile Engineering, 2000. **Volume 214**(Volume 214, Number 7 / 2000): p. 705-717.
29. Daowei, Z. and X. Hui. *Control Strategy Optimization of the Hybrid Electric Bus Based on Remote Self-Learning Driving Cycles*. in *IEEE Vehicle Power and Propulsion Conference (VPPC)*. 2008. Harbin, China.

30. Lin, C.-C., et al., *Control System Development for an Advanced-Technology Medium-Duty Hybrid Electric Truck*. 2003: SAE International.
31. Sill, J., S. Molla, and B. Ayalew, *Modeling and Control of Handling Dynamics for a Hydrostatically Driven Vehicle.* International Journal of Heavy Vehicle Systems, 2010.
32. McCandlish, D. and R.E. Dorey, *The Mathematical Modeling of Hydrostatic Pumps and Motors.* Proceeding of Inst. Mech. Engineers. Part B. , 1984. **Vol. 198**(10): p. 165-174.
33. Pease, G., and Henderson, Jerald H., *Simulation of a Hydraulic Hybrid Vehicle Using Bond Graphs.* Transactions of ASME, Journal of Mechanisms, Transmissions, and Automation in Design, 1988. **Vol.110**: p. 365-369.
34. Wilson, W.E., *Rotary-Pump Theory.* ASME Transactions, 1946. **Vol. 68**(4): p. 371-384.
35. www.Tobul.com. *http://www.ahscorp.net/Individual%20Prod%20Images/Accumulators/Bladder%20Accum.pdf*. 2010 [cited 2010.
36. Pourmovahed, A., N.H. Beachley, and F.J. Fronczak, *Modeling of a Hydraulic Energy Regeneration System- Part I: Analytical Treatment.* Transactions of ASME, Journal of Dynamic Systems, Measurement and Control, 1992. **Vol. 114**: p. 155-159.
37. Pourmovahed, A., *An experimental thermal time constant correlation for hydraulic accumulators.* Transactions of ASME, Journal of Dynamic Systems, Measurement and Control, 1990. **Vol. 112**: p. 116-121.
38. Cengel, Y.A. and M.A. Boles, *Thermodynamics: An Engineering Approach, 5th Edition*. 2005: McGraw Hill.
39. Watton, J., *Fluid Power Systams: modeling, simulation, analog and microcomputer control*. 1989: Prentice Hall International(UK) LTD.
40. Ayalew, B. and B.T. Kulakowski, *Modal Approximation of Distributed Dynamics for a Hydraulic Transmission Line with Pressure Input -Flow Rate Output Causality.* Transactions of the ASME, Journal of Dynamic Systems Measurement and Control, 2005. **Vol. 127**.
41. Cross, P.W., *System Modeling and Energy Management Strategy Development for Series Hybrid Vehicles*, in *George W. Woodruff School of Mechanical Engineering*. 2008, Georgia Institute of Technology. p. 133.
42. Kirk, D.E., *Optimal Control Theory: An Introduction*. 1970, Mineola, New York: Dover Publications, Inc.
43. Bellman, R., E., *Dynamic Programming*. 1957: PrincetonUniversity Press, New Jersey.
44. Sciarretta, A. and L. Guzzella, *Control of Hybrid Electric Vehicles: Optimal Energy Managment Strategies*, in *IEEE Control Systems Magazine*. 2007. p. 60-70.
45. Pisu, P. and G. Rizzoni. *A Supervisory Control Strategy for Series Hybrid Electric Vehicles with two energy storage systems*. in *Vehicle Power and Propulsion Conference 2005*. 2005. Chicago, IL.

46. Paganelli, G., Y. Guezennec, and G. Rizzoni, *Optimizing Control Strategy for Hybrid Fuel Cell Vehicle*, in *SAE World Congress*. 2002: Detroit, Michigan.